Adverse roles of mast cell chymase-1 in COPD

EUROPEAN RESPIRATORY *journal*

FLAGSHIP SCIENTIFIC JOURNAL OF ERS

Early View

Original research article

Adverse roles of mast cell chymase-1 in chronic obstructive pulmonary disease

Gang Liu, Andrew G. Jarnicki, Keshav R. Paudel, Wenying Lu, Ridhima Wadhwa, Ashleigh M. Philp, Hannelore Van Eeckhoutte, Jacqueline E. Marshall, Vamshikrishna Malyla, Angelica Katsifis, Michael Fricker, Nicole G. Hansbro, Kamal Dua, Nazanin Z. Kermani, Mathew S. Eapen, Angelica Tiotiu, K. Fan Chung, Gaetano Caramori, Ken Bracke, Ian M. Adcock, Sukhwinder S. Sohal, Peter A. Wark, Brian G. Oliver, Philip M. Hansbro

Please cite this article as: Liu G, Jarnicki AG, Paudel KR, *et al*. Adverse roles of mast cell chymase-1 in chronic obstructive pulmonary disease. *Eur Respir J* 2022; in press (https://doi.org/10.1183/13993003.01431-2021).

Adverse roles of mast cell chymase-1 in chronic obstructive pulmonary disease

Gang Liu[1], Andrew G. Jarnicki[2], Keshav R. Paudel[1], Wenying Lu[3], Ridhima Wadhwa[1], Ashleigh M. Philp[1,4], Hannelore Van Eeckhoutte[5], Jacqueline E Marshall[1], Vamshikrishna Malyla[1], Angelica Katsifis[1], Michael Fricker[6], Nicole G. Hansbro[1], Kamal Dua[1,7], Nazanin Z. Kermani[8], Mathew S. Eapen[3], Angelica Tiotiu[9,10], K. Fan Chung[9], Gaetano Caramori[11], Ken Bracke[5], Ian M. Adcock[9], Sukhwinder S. Sohal[3], Peter A. Wark[6], Brian G. Oliver[12], Philip M. Hansbro[1,6*]

[1]Centre for Inflammation, Centenary Institute and University of Technology Sydney, School of Life Sciences, Faculty of Science, Sydney, New South Wales, Australia

[2]Department of Pharmacology and Therapeutics, University of Melbourne, Parkville, Victoria, Australia

[3] Respiratory Translational Research Group, Department of Laboratory Medicine, School of Health Sciences, University of Tasmania, Launceston, Tasmania 7248, Australia

[4]St Vincent's Medical School, University of New South Wale Medicine, University of New South Wale, Sydney, New South Wales, Australia

[5]Laboratory for Translational Research in Obstructive Pulmonary Diseases, Department of Respiratory Medicine, Ghent University Hospital, Ghent, Belgium.

[6]Priroity Research Centre for Healthy Lungs, Hunter Medical Research Institute, University of Newcastle, New South Wales, Australia

[7]Discipline of Pharmacy, Graduate School of Health, University of Technology Sydney, Ultimo, NSW, Australia

[8]Data Science Institute, Department of Computing, Imperial College London, United Kingdom

[9]National Heart & Lung Institute, Imperial College London, United Kingdom

[10]Department of Pulmonology, University Hospital of Nancy, France

[11]UOC di Pneumologia, Dipartimento di Scienze Biomediche, Odontoiatriche e delle Immagini Morfologiche e Funzionali (BIOMORF), Università di Messina, Italy.

[12]Woolcock Institute and School of Life Science, Faculty of Science Life science, University of Technology Sydney, Sydney, New South Wales, Australia

[*]Correspondence to: Professor Philip M Hansbro, Centre for Inflammation, Centenary Institute, Building 93, Royal Prince Alfred Hospital, John Hopkins Drive, Camperdown, NSW 2050, Australia. Email: philip.hansbro@uts.edu.au

Take home message

hCMA1 that released from mast induces macrophages to release TNF-α in the lung and promotes the pathogenesis of COPD. hCMA1 may be a novel therapeutic target in COPD.

Running title: CMA1-dependent COPD

Word count: 4,098 Max 3,000.

Abstract

Background. COPD is the third leading cause of death worldwide. Cigarette smoke (CS)-induced chronic inflammation inducing airway remodelling, emphysema and impaired lung function is the primary cause. Effective therapies are urgently needed. Human chymase-1 (hCMA1) and it's ortholog mCMA1/mouse mast cell (MC) protease-5 (mMCP5) are exocytosed from activated MCs and have adverse roles in numerous disorders, but their role in COPD is unknown.

Methods. We evaluated hCMA1 levels in lung tissues of COPD patients. We used *mmcp5*-deficient ($^{-/-}$) mice to evaluate this proteases' role and potential for therapeutic targeting in CS-induced experimental COPD. We also used *ex vivo/in vitro* studies to define mechanisms.

Results. The levels of hCMA1 mRNA and $CMA1^{+}$ MCs were increased in lung tissues from severe compared to early/mild COPD patients, non-COPD smokers and healthy controls. Degranulated MC numbers and mMCP5 protein were increased in lung tissues of wild-type (WT) mice with experimental COPD. *mmcp5*$^{-/-}$ mice were protected against CS-induced inflammation and macrophage accumulation, airway remodelling, emphysema and impaired lung function in experimental COPD. CS extract challenge of co-cultures of MCs from WT but not *mmcp5*$^{-/-}$ mice with WT lung macrophages increased in TNF-α release. It also caused the release of CMA1 from human MCs, and recombinant hCMA-1 induced TNF-α release from human macrophages. Treatment with CMA1 inhibitor potently suppressed these hallmark features of experimental COPD.

Conclusion. CMA1/mMCP5 promotes the pathogenesis of COPD, in part, by inducing TNF-α expression and release from lung macrophages. Inhibiting hCMA1 may be a novel treatment for COPD.

250 words, Max: 250 words

Keywords

COPD, mast cell, chymase-1, mMCP5, TNF-α

Introduction

Chronic obstructive pulmonary disease (COPD) affects >300 million people globally [1]. Cigarette smoke (CS)-induced chronic inflammation is the major cause, however, air pollution, bushfire smoke, and genetic factors contribute [2]. Pulmonary inflammation in COPD is characterised by increased neutrophils, macrophages, lymphocytes and mast cells (MCs). These changes lead to small airway remodelling and alveolar destruction and emphysema [3], airflow limitation, impaired lung function and severe breathing difficulties often leading to death [4]. Current treatments aim to reduce symptoms and do not halt or reverse the progression of COPD. A deeper understanding of pathogenesis will enable the identification of new therapeutic targets, and the development of new therapies.

MCs are potent multifunctional immune cells that reside in the lung and other organs. MC-committed progenitors are generated in the bone marrow and foetal liver. They reach their target organs *via* the circulation where they complete their differentiation and maturation [5]. MCs are major contributors to innate and acquired immunity [5], and are first-line responders to insults like CS [6]. MC secretory granules contain pre-formed mediators, including tryptases and chymases that have potent immune bioactivities. Exposure to foreign particles induce MCs to degranulate and release their pre-formed pro-inflammatory mediators [7]. We previously demonstrated adverse roles for MCs and their granule tryptases in the pathogenesis of CS-induced experimental COPD [8-11]. Another prominent protease in human (h)MCs is chymase-1 (hCMA1, GenBank GeneID 1215) [12]. The Human and Mouse Genome Consortia concluded mouse MC protease (mMCP)5 (mMCP5, Gene ID 17226) is the ortholog of hCMA1 [13], even though mouse MCs express additional related proteases [14]. Furthermore, mCMA1/mMCP-5 is packaged in granules of mMCs with heparin proteoglycans and mouse carboxypeptidase-A3 (mCPA3), as is hCMA1 in hMCs.

Mouse and human CMA1 have important roles in numerous inflammatory disorders, including cardiovascular and pulmonary diseases [15]. hCMA1 can mediate the conversion of angiotensin (Ang)-I to Ang-II, and inhibiting Ang-II reduces blood pressure and protects against cardiovascular and metabolic disorders [15]. Increased numbers of MCs occur in the lung fluids and tissues of COPD patients [16]. hCMA1^{+} MCs are increased in the lungs of severe (Global Initiative for Chronic Obstructive Lung Disease [GOLD] IV) COPD patients [17]. Inhibiting mouse chymases reduced pulmonary hypertension and fibrosis in an experimental model of lung injury [18]. Nevertheless, the roles of mouse and human CMA1 in COPD is unknown.

We show that hCMA1 transcripts and CMA1^{+} MCs are increased in bronchial biopsies and lung tissues from COPD patients compared to controls. We demonstrate that our *mmcp5*-deficient ($^{-/-}$) mice are protected against the development of CS-induced experimental COPD. We also show that CS extract (CSE) induces mMCP5/CMA1 release from MCs that promotes macrophage lung accumulation and tumour necrosis factor (TNF)-α production from mouse and human cells. Pharmacological inhibition of mCMA1/mMCP5 suppressed the hallmark features of experimental COPD suggesting that targeting hCMA1 may be therapeutically beneficial.

Methods

Detailed descriptions are as previously described and in the online supplement [3, 8, 10-12, 19-25]

Results

Chymase 1 (CMA1) mRNA levels are increased in the lungs of COPD patients

To define the role of hCMA1 in COPD, we first assessed its mRNA levels in bronchial biopsies from mild COPD patients (GOLD I-II), non-COPD smokers, and non-smoking healthy controls in an existing dataset (GSE8545) [26]. Levels were not significantly different between groups (**figure 1a**). However, in another microarray dataset (GSE5058) [27] *hCMA1* mRNA levels were significantly increased in severe COPD patients (GOLD III-IV) compared to both non-COPD smokers (P=0.011) and healthy controls (P=0.049, **figure 1b**). To confirm the association with severe rather than mild COPD, we next assessed levels in lung biopsies from lung healthy and non-COPD smoker controls and mild (GOLD I-II) and severe (III-IV) COPD patients in another larger validation dataset (GSE37147) [28]. *hCMA1* mRNA levels were again not different in mild but were significantly increased in severe COPD patients compared to controls (P=0.017, **figure 1c**). *hCMA1* mRNA levels were significantly increased in lung tissues from severe COPD patients (combined GSE38974 and GSE69818), there was no difference between GOLD III and IV (**figure 1d**).

MCs and CMA1$^+$ MCs are increased in the lungs of COPD patients

MC gene signatures derived from single cell (sc)RNA-seq analysis [29, 30] were enriched in COPD lung tissue compared to healthy control subjects and reached significance in GOLD stage 4 subjects (p=0.04, **Supplementary table 2**). Previous data suggests that this reflects more MCs in asthmatic bronchial biopsy tissue than in healthy control tissue [29]. There was also a significant correlation between the enrichment scores for these scRNA-seq MC signatures and CMA1 expression according to GOLD stage (**figure 1e**).

To validate the increases in CMA1 expression in lung tissue, we measured its' transcript levels in lung samples by qPCR. We found that CMA1 mRNA levels were significantly increased in lung samples from COPD GOLD stage II-IV patients compared to never smokers (**figure 1f and Supplementary table 3**). Several previous studies showed that

hCMA1^{+} MCs are increased in lungs from COPD patients compared to healthy donors [17, 31]. Notably, we confirmed this by immunohistochemistry and showed that CMA1^{+} MCs were significantly increased in lung tissues from COPD patients (**figure 1g**) compared to lung healthy controls (**figure 1h**).

Degranulated MCs and mMCP5 protein are increased in the lungs in CS-induced experimental COPD

We next used our well-established nose-only CS-induced experimental model of COPD to examine the role of mCMA1/mMCP5 in pathogenesis [3, 8-11, 21]. Lungs were collected from wild-type (WT) C57BL/6 mice after 8 weeks of CS exposure, when the major hallmark features of human COPD (chronic airway inflammation, airway remodelling/fibrosis, emphysema-like alveolar enlargement, impaired lung function) have developed. The levels of CS exposure are representative of a pack-a-day human smoker. Lung sections were stained with chloroacetate esterase to detect activated MCs that had degranulated (**figure 2a**). MC numbers were substantially increased (>3-fold) after 8 weeks of CS exposure compared to normal air-exposed controls (**figure 2a and b**). These MCs showed more degranulation when exposed to CS (**figure 2c**). MCs were localised in the lung parenchyma of control mice, but these cells (degranulated MCs) were located close to blood vessels and airways in experimental COPD (**Supplementary figure 1**). The levels of mCMA1/mMCP5 gene (**Supplementary figure 2a**) and protein (**figure 2d and e**) were significantly increased in the lungs in experimental COPD. CS exposure increased mMCP5^{+} and mMCP6^{+} MCs in the lungs in experimental COPD, with greater increases in mMCP5^{+} MCs (**figure 2f–h**). These cells also shifted from the parenchyma to connective tissues close to blood vessels and airways after 8 weeks CS exposure. There are 5 chymase paralogs in mice and *mcpt* is the gene name for mMCPs. The sequence for *mcpt3* does not exist, and so we assessed the

expression of the others (*mcpt1/2/4*) in the lungs in experimental COPD. CS exposure increased *mcpt1* mRNA transcript levels but did not change those of *mcpt2* and *mcpt4* (**supplementary figure 2b–d**). *mcpt5* gene expression was also increased in mouse livers after 8 weeks of CS exposure but *mmcpt2* and *4* levels were unchanged (**Supplementary figure 2e–g**).

Generation of mmcp5$^{-/-}$ C57BL/6 mice

Transgenic *mmcp5*$^{-/-}$ mice were generated by replacing intron 2 and exon 3 of the *mmcp5* gene with the Neo^{r} gene [12]. We further characterised these mice by showing that the exon 3 DNA fragment of the *mmcp5* gene in *mmcp5*$^{-/-}$ mice was larger than in WT mice due to the insertion of the Neo^{r} gene (**figure 3a**). We also showed that mMCP5 protein was detectable in lung extracts from WT but not *mmcp5*$^{-/-}$ mice by immunoblot (**figure 3b and Supplementary figure 3a**). We also isolated and cultured mBMMCs from WT and *mmcp5*$^{-/-}$ mice and confirmed their identity with chloroacetate esterase staining (**figure 3c**). mBMMCs from WT but not *mmcp5*$^{-/-}$ mice, contained mMCP5 protein (**figure 3d**). Furthermore, mMCP5 protein was detected in mBMMC lysates from WT but not *mmcp5*$^{-/-}$ mice (**figure 3e and Supplementary figure 3b**).

mmcp5$^{-/-}$ mice have reduced pulmonary macrophages in experimental COPD

We next assessed pathogenesis in the lungs in WT compared to *mmcp5*$^{-/-}$mice exposed to CS for 8 weeks. BALF was collected and total and differential leukocyte counts determined. WT mice had increased numbers of total leukocytes in experimental COPD compared to normal air-exposed controls. In contrast, *mmcp5*$^{-/-}$ mice had significantly reduced total leukocytes compared to WT mice with experimental COPD, although numbers were still higher than air-exposed WT and *mmcp5*$^{-/-}$ controls (**figure 4a**). Differential counts showed that macrophages,

neutrophils and lymphocytes were the predominant cells and were increased in the airways of WT mice with experimental COPD. The reduced total leukocytes in the BALF of CS-exposed *mmcp5*$^{-/-}$ mice was due primarily to reduced numbers of macrophages (~50%) with no change in other leukocytes. We previously showed that macrophages are critical in experimental COPD pathogenesis and their depletion suppressed disease development [8]. We also found that MC numbers were increased in the lungs from WT and *mmcp5*$^{-/-}$ mice but were not different between the two strains (**Supplementary figure 4**).

mmcp5$^{-/-}$ *mice have reduced pulmonary TNF-α protein levels in experimental COPD*

We next assessed the mRNA levels of key pathogenic cytokines and chemokines in mouse lungs using RT-qPCR. *Tnfa* mRNA levels were significantly increased in the lungs of WT mice with experimental COPD compared to normal air-exposed controls (**figure 4b**). In contrast, CS- and air-exposed *mmcp5*$^{-/-}$ mice had substantially lower levels of *Tnfa* mRNA that were below baseline expression in air-exposed WT mice. In contrast, lung *Cxcl1* mRNA levels were significantly increased and similar between WT and *mmcp5*$^{-/-}$ mice after 8 weeks of CS exposure (**figure 4c**). CS exposure did not change the mRNA expression of other factors important in COPD, MC responses and macrophage recruitment; transforming growth factor-β (*Tgfb1*), *Il33*, *Ccl2* and *Il12* in the lungs of WT or *mmcp5*$^{-/-}$ mice (**figure 4d-g**). We also determined TNF-α protein levels by ELISA. CS exposure-induced increased TNF-α protein levels in the lungs of WT and *mmcp5*$^{-/-}$ mice compared to air-exposed controls (**figure 4h**). However, the levels were significantly reduced in CS-exposed *mmcp5*$^{-/-}$ compared to WT mice.

mmcp5$^{-/-}$ *mice have reduced small airway remodelling in experimental COPD*

Small airway remodelling is a major intractable feature of COPD. To explore the role of mMCP5 in this process, lung sections from WT and *mmcp5*$^{-/-}$ mice were stained with Masson's trichrome to evaluate histochemically small airways collagen deposition (**figure 5a**). Collagen deposition was significantly increased around small airways in WT mice with experimental COPD compared to normal air-exposed controls (**figure 5b**). In contrast, *mmcp5*$^{-/-}$ mice were completely protected against airway fibrosis with levels comparable to baseline in air-exposed controls. CS exposure resulted in epithelial cell thickening in small airways from WT mice (**figure 5c**). However, the absence of mMCP5 protected against epithelial thickening after 8 weeks of CS exposure (**figure 5d**). CS exposure increased mucus cells around the airways, but the numbers were not different between WT and *mmcp5*$^{-/-}$ mice (**Supplementary figure 5**).

mmcp5$^{-/-}$ *mice have reduced emphysema in experimental COPD*

Emphysema is another major intractable feature and critical disease issue in COPD. To assess the role of mMCP5 alveolar diameter was measured to assess emphysema-like enlargement in WT and *mmcp5*$^{-/-}$ mice (**figure 5e**). Eight weeks of CS exposure increased alveolar diameter in WT mice (**figure 5f**). In contrast, *mmcp5*$^{-/-}$ mice were completely protected against CS-induced alveolar enlargement with significantly lower airspace diameter compared to CS-exposed WT mice, with levels similar to baseline in air-exposed controls. Matrix metalloproteinases (MMPs) regulate ECM degradation that contributes to airway remodelling and emphysema in COPD [32]. CS exposure increased pro- and active-MMP9 proteins in WT mouse lungs that was absent in *mmcp5*$^{-/-}$ mice (**figure 5g–i**).

mmcp5$^{-/-}$ *mice are protected against impaired lung function in experimental COPD*

We next assessed whether the combined effects of reduced pathogenic features affected lung function in *mmcp5*$^{-/-}$ mice. Lung function, in terms of transpulmonary resistance (**figure 6a**), lung volume (**figure 6b**) and dynamic compliance (**figure 6c**) were all increased in WT mice with experimental COPD compared to air-exposed controls. These changes were completely inhibited in *mmcp5*$^{-/-}$ mice after CS exposure and were at baseline levels in air-exposed controls. We also measured static lung compliance to assess lung elasticity using pressure-volume loops (**figure 6d**). Static lung compliance was increased in WT mice with experimental COPD and was comparatively decreased in CS-exposed *mmcp5*$^{-/-}$ mice.

mMCP5 promotes MC-induced macrophage production of TNF-α with CSE challenge

We then assessed how mCMA1/mMCP5 contributes to experimental COPD pathogenesis. *mmcp5*$^{-/-}$ mice had reduced lung TNF-α mRNA and protein levels after 8 weeks of CS exposure (**figure 4**). Although MCs can transiently express TNF-α, macrophages are the main cellular source in the lung [33]. TNF-α has major roles in COPD pathogenesis, and inhibiting its receptors reduces inflammation and emphysema in an experimental model of CS-induced COPD [34]. To further define how MCs and mCMA1/mMCP5 promotes TNF-α production in COPD, we generated mouse bone marrow-derived MCs (mBMMCs) from naïve WT and *mmcp5*$^{-/-}$mice (**figure 3a**). *Ex vivo* differentiated mBMMCs from WT mice contained mMCP5 protein, whereas those from *mmcp5*$^{-/-}$ mice did not (**Figure 3d–e**), further confirming the genotype data (**figure 3a**).

Exposure of macrophages to 5% CSE causes the secretion of TNF-α protein, but this concentration does not affect MC viability [35]. We, therefore, chose this concentration of CSE for our studies. To identify the optimal timepoint for CSE exposure of mBMMCs, lung macrophages (Raw246.7) were co-cultured with or without WT mBMMCs over a 6-48h

time-course of 5% CSE challenge. TNF-α protein levels were measured in lysates by ELISA (**Supplementary figure 6**). Macrophages secreted more TNF-α protein (p=0.071) when co-cultured with WT mBMMCs after 12h of 5% CSE challenge, with a significant increase and peak after 24h (**figure 7a**). TNF-α levels were not changed at early (6h) or later (48h) time points. We, therefore, selected 24h as the optimal time point. Macrophages and mBMMCs from WT and *mmcp5*$^{-/-}$ mice were co-cultured with or without 5% CSE challenge for 24h, and TNF-α proteins were measured in lysates by ELISA. Macrophages co-cultured with mBMMCs from WT mice and exposed to CSE released substantially increased levels (2-fold) of TNF-α compared to media exposure (**figure 7b**). In contrast, co-cultures with mBMMCs from *mmcp5*$^{-/-}$ mice exposed to CSE did not produce increased TNF-α relative to media-treated controls with levels substantially reduced compared to WT mBMMCs. mCMA1/mMCP5 is, therefore, critical for TNF-α production by macrophages in response to CS. We also found that CSE-induced TNF-α protein was reduced in cell supernatants after co-culture with BMMCs from *mmcp5*$^{-/-}$ mice (**figure 7c**).

To further define the role mMCP5 in COPD, we assessed the responses of primary alveolar macrophages (**Supplementary figure 7**) from WT and *mmcp5*$^{-/-}$ mice challenged with CSE. TNF-α protein levels were significantly increased in macrophages from both WT and *mmcp5*$^{-/-}$ mice after challenge (**figure 7d**). Then WT alveolar macrophages were co-cultured with BMMCs from WT and *mmcp5*$^{-/-}$ mice with or without CSE. CSE induced TNF-α protein responses in macrophages co-cultured with WT but not *mmcp5*$^{-/-}$ BMMCs (**figure 7e**).

CSE challenge also increased CMA1 protein levels in human MCs (**figure 7f**) cell supernatant (**figure 7g**). Furthermore, recombinant hCMA1 protein increased TNF gene expression (**figure 7h**) and protein levels in supernatants of human macrophages (**figure 7i**).

These findings confirmed the mechanism whereby CS induced CMA1 release from MCs that increased TNF production by macrophages (**figure 7g**).

Therapeutic inhibition of CMA1 in mice reduces inflammation, small airway remodelling, emphysema and impaired lung function in experimental COPD

BMMCs from WT mice were co-cultured with macrophages. Cell were challenged with 5% CSE and treated with CMA1 inhibitor. Substantial increases in CSE-induced TNF protein levels in cell lysates were completely inhibited with CMA1 inhibitor treatment (**figure 8a**). We then treated mice with a CMA1 inhibitor between 6-8 weeks of CS exposure to test the therapeutic potential. The CMA1 inhibitor had potent effects and suppressed all of the hallmark features of experimental COPD. Treatment suppressed chronic airway inflammation and reduced total leukocytes, predominantly macrophages, neutrophils and lymphocytes in BALF after 8 weeks CS exposure (**figure 8b-e**). Treatment also almost completely suppressed airway fibrosis and collagen deposition around the small airways (**figure 8f and g**) and emphysema-like alveolar enlargement (**figure 8h and i**) back to baseline in air-exposed controls in both cases. Treatment also prevented decreases in lung function in terms of lung volume, dynamic compliance and static lung compliance (**figure 8j–l**) again back to baseline levels in air-exposed controls.

Discussion

We show for the first time that MC-derived CMA1/mMCP5 contributes to COPD pathogenesis. *hCMA1* mRNA is expressed at higher levels and $CMA1^+$ MCs are increased in the lungs of COPD patients. Lung mCMA1/mMCP5 protein, MCs and $mMCP5^+$ MCs are increased in experimental COPD. We developed *mmcp5*$^{-/-}$ mice and showed that mMCP5 has a prominent deleterious role in experimental COPD. *mmcp5* deficiency protects against

pulmonary inflammation, airway remodelling, emphysema, and impaired lung function in experimental COPD. Notably, treatment with a CMA1 inhibitor potently suppressed these hallmark features of experimental COPD. Finally, we define the mechanism whereby CS induces CMA1 release that in turn induces TNF-α secretion from macrophages.

COPD is a progressive disease, and CS-induced inflammation is a primary driver of pathogenesis. MCs have potent effects on immunity through degranulation and secretion of potent mediators; chymases, tryptases and others. They have important roles in lung disorders, particularly asthma, and we now show in COPD. We are the first to show increased *hCMA1* mRNA expression in lung biopsies from severe COPD patients, indicating that it is associated with increased disease severity. Previous studies showed that hCMA1^{+} MCs are increased in COPD lungs compared to healthy donors [17, 31]. Some reported that they are resident around blood vessels [17], whereas others showed that they were mainly located around airway smooth muscle in COPD lungs [31].

We found that degranulated MCs were also increased in the lungs of WT mice with CS-induced experimental COPD, confirming that pulmonary MC are activated. We also found increased mMCP5 protein levels in experimental COPD lungs, in line with increased *hCMA1* mRNA levels and CMA1^{+} MCs in patient lungs. We also found that CMA1^{+} MCs were in the parenchyma in controls but around blood vessels and airways in experimental COPD.

Using *mmcp5*$^{-/-}$ C57BL/6 mice, we demonstrate critical roles for mMCP5 in experimental COPD through driving pulmonary macrophage and TNF-α responses. We previously showed that *mmcp5*$^{-/-}$ mice have reduced pathology in experimental arthritis [12], supporting our current findings that mMCP5 regulates MC-dependent inflammation. MCs express a diverse array of pro- and anti-inflammatory responses. Our previous studies revealed that MCs have potent pro-inflammatory activity in response to particulate insults.

Mice deficient in other MC proteases (e.g. mMCP6 homologue of human tryptase-β, and Prss31 homologue of human tryptase-γ) were partially protected from inflammation and small airway remodelling in experimental CS-induced COPD [9]. However, other studies show that MCs can suppress inflammation in other contexts [36]. MCs protect mice against bacterial and viral infection and *Mycoplasma pulmonis*-induced pneumonia, and infected MC-deficient mice die due to a lack of protective immunity [37].

We confirmed that lung TNF-α mRNA expression and protein levels are increased in CS-induced experimental COPD and show critical roles for mMCP5 in driving these responses using *mmcp5*$^{-/-}$ mice. Previous studies show TNF-α protein was increased in macrophages after CSE challenge [38]. In this study, TNF-α protein levels were also increased in co-cultured macrophages after CSE challenge. We also show that this TNF-α protein release from macrophages was increased after co-culture with MCs from WT but not *mmcp5*$^{-/-}$ mice when exposed to CSE. TNF-α is an important pro-inflammatory cytokine in COPD with critical roles in inflammatory cell recruitment and tissue remodelling [39]. TNF-α mRNA and protein levels are increased in COPD patients, and macrophages are the primary lung cell source [33]. Together these findings provide strong evidence that mMCP5 regulates TNF-α production from macrophages in experimental COPD. Further studies are needed to define the molecular mechanisms involved and the contributions of other myeloid cells.

The reduction in inflammatory responses in *mmcp*$^{-/-}$ mice resulted in the complete inhibition of airway fibrosis and emphysema. Further studies need to deduce how mMCP5 promotes these effects. h/mCMA1 and h/mCPA3 are stored in the secretory granules of MCs in a 1:1 ratio. This is because pro-mCMA1/pro-mMCP5 forms a binary complex in the endoplasmic reticulum of MCs. Thus, target disruption of the *mmcp5* gene adversely impacts

the levels of mCPA3 in murine MCs [12]. It is therefore possible that mMCP5 participates indirectly in experimental COPD by reducing mCPA3 protein levels in pulmonary MCs.

Previous studies demonstrated that MCs increase collagen production by inducing lung fibroblast proliferation [40] leading to small airway remodelling in COPD [9]. We previously showed that ischemia-reperfusion injury of skeletal muscle is reduced in *mmcp5*$^{-/-}$ compared to WT mice, further supporting prominent roles for CMA1/mMCP5 in connective tissue remodelling [41]. TNF-α contributes to lung remodelling and tissue repair and induces collagen synthesis [42]. The lack of TNF-α in *mmcp5*$^{-/-}$ mice prevents collagen deposition around the small airways. However, mMCP5 also regulates the expression and processing of certain matrix metalloprotease (MMPs) zymogens that control the deposition and cleavage of collagen and other remodelling proteins. mMCP5 has similar functional roles in inducing tissue damage in the skin. Tight junctions are decreased in *mmcp5*$^{-/-}$ mice in an experimental model of thermal skin injury compared to WT mice [43]. MMPs also contribute to tissue destruction in the lungs by cleaving structural proteins leading to emphysema [32]. We previously showed that compound 48/80-induced MC degranulation results in an increase of MMP-9 protein in the peritoneal cavity of WT mice, but this is reduced in *mmcp5*$^{-/-}$ mice [12]. In this study, we also found CS-induced increases in pro- and active MMP9 protein in WT mice that was prevented by the absence of mMCP5. These data suggest that mMCP5 contributes to MMP activation to induce fibrosis and emphysema and its inhibition may protect against these pathogenic features.

Lung function measurements are used to identify structural and functional changes in COPD patients. We established that increased transpulmonary resistance, lung volume and compliance occur in experimental COPD [3]. *mmcp5*$^{-/-}$ mice were protected against CS-induced transpulmonary resistance and compliance, which further confirm protection against small airway remodelling and emphysema, respectively. Increased lung volumes are

associated with emphysema that result from the destruction of alveolar walls [44]. Transpulmonary resistance is a measure of airway and lung constriction. Small airway remodelling and alveolar wall thickening increase transpulmonary resistance [45]. Dynamic compliance is a measure of airways and parenchyma elasticity and lung distention during breathing [46]. Static compliance reflects the elasticity of the parenchyma [47].

Previous studies show that the CMA1 inhibitor (RO5066852) reduced atherosclerotic plaque progression [48], but the effect of this inhibitor has not been tested in lung diseases. We are the first to show that this pharmaceutical CMA1 inhibitor potently reduces inflammation, small airway remodelling, emphysema and improved lung function in an experimental model of CS-induced COPD in mice. We also show that this CMA1 inhibitor reduces MCs induced TNF protein after CSE challenge, indicating CMA1 is a potential therapeutic target and that inhibitors could be a potential treatment for COPD.

Tryptases are serine proteinases. Tetramer-forming hTryptase-β and membrane hTryptase-γ are the most abundant in hMCs [49]. We previously showed that TNF-α protein levels were increased in lysates of bone marrow-derived macrophages exposed to recombinant hTryptase-β [8]. We also showed that *mmcp6*$^{-/-}$mice had reduced airway inflammation and lung *Tnfa* mRNA levels compared to WT mice in CS-induced experimental COPD [8]. Furthermore, *Prss31*$^{-/-}$ mice had significantly reduced CS-induced airway inflammation and remodelling [9].

Collectively, this and previous studies show that several MC granule proteases have potent adverse effects in driving disease. It is important to define which are more significant in a particular disease and develop specific inhibitors against them as therapies. It may be necessary to suppress multiple proteases, which could be achieved with either combination therapies, inhibitors of MC degranulation or modifying the serglycin proteoglycans needed to maintain MC proteases in active conformations in order to function. These issues should be

elucidated in future studies. Nevertheless, we show potent effects of specifically inhibiting mCMA1/mMCP5 in the suppression of the hallmark features of experimental COPD. We show that CS increases MC numbers and degranulation to release mMCP5. mMCP5 then induces macrophages to release TNF-α in the lung, leading to inflammation, airway remodelling, emphysema and impaired lung function in COPD (**figure 7j**). Inhibiting mMCP5 levels and activity reduces lung inflammation, airway remodelling, emphysema and impaired lung function. Inhibiting hCMA1 may be a new therapeutic option for COPD.

ACKNOWLEDGEMENTS

PMH is supported by a fellowship and grants from the National Health and Medical Research Council of Australia (NHMRC #1079187, #1175134), Australian Research Council (#150102153), and the University of Technology Sydney. GL is supported by CREATE Hope Scientific Fellowship. We thank Duc Nguyen, Nisha Panth and Christina Nalkurthi for technical assistance. We thank Roche for permission to use and provision of RO5066852-000-006.

AUTHOR CONTRIBUTIONS

G.L performed most of the *in vitro* and *in vivo* experiments. K.R.P, A.M.P, A.G.J, M.F and K.D performed *in vivo* experiments. W.L, M.S.E and S.S.S performed human immunohistochemistry. R.W and V.M assisted *in vitro* experiments. H.V.E, K.B performed qPCR in human samples. J.E.M assisted immunoblot. A.K assisted qPCR in mice. N.Z.K and I.M.A performed sc-RNA seq analysis. K.F.C, G.C, A.T and I.M.A assisted in dataset analysis. G.L. P.M.H designed the experiments. P.J.H, P.A.W and B.G.O revised the manuscript. P.M.H funded the experiments. All authors read and approved the manuscript.

CONFLICT OF INTEREST

The authors declare that the research was conducted in the absence of any commercial or financial relationships that could be construed as a potential conflict of interest.

REFERENCES

1. Collaborators GBDCRD. Prevalence and attributable health burden of chronic respiratory diseases, 1990-2017: a systematic analysis for the Global Burden of Disease Study 2017. *Lancet Respir Med* 2020: 8(6): 585-596.
2. Budden KF, Gellatly SL, Wood DL, Cooper MA, Morrison M, Hugenholtz P, Hansbro PM. Emerging pathogenic links between microbiota and the gut-lung axis. *Nat Rev Microbiol* 2017: 15(1): 55-63.
3. Liu G, Cooley MA, Jarnicki AG, Hsu AC, Nair PM, Haw TJ, Fricker M, Gellatly SL, Kim RY, Inman MD, Tjin G, Wark PA, Walker MM, Horvat JC, Oliver BG, Argraves WS, Knight DA, Burgess JK, Hansbro PM. Fibulin-1 regulates the pathogenesis of tissue remodeling in respiratory diseases. *JCI Insight* 2016: 1(9).
4. Budden KF, Shukla SD, Rehman SF, Bowerman KL, Keely S, Hugenholtz P, Armstrong-James DPH, Adcock IM, Chotirmall SH, Chung KF, Hansbro PM. Functional effects of the microbiota in chronic respiratory disease. *Lancet Respir Med* 2019: 7(10): 907-920.
5. Krystel-Whittemore M, Dileepan KN, Wood JG. Mast Cell: A Multi-Functional Master Cell. *Front Immunol* 2015: 6: 620.
6. Wang Y, Xu J, Meng Y, Adcock IM, Yao X. Role of inflammatory cells in airway remodeling in COPD. *Int J Chron Obstruct Pulmon Dis* 2018: 13: 3341-3348.
7. Hamilton MJ, Frei SM, Stevens RL. The multifaceted mast cell in inflammatory bowel disease. *Inflamm Bowel Dis* 2014: 20(12): 2364-2378.
8. Beckett EL, Stevens RL, Jarnicki AG, Kim RY, Hanish I, Hansbro NG, Deane A, Keely S, Horvat JC, Yang M, Oliver BG, van Rooijen N, Inman MD, Adachi R, Soberman RJ, Hamadi S, Wark PA, Foster PS, Hansbro PM. A new short-term mouse model of chronic obstructive pulmonary disease identifies a role for mast cell tryptase in pathogenesis. *J Allergy Clin Immunol* 2013: 131(3): 752-762.
9. Hansbro PM, Hamilton MJ, Fricker M, Gellatly SL, Jarnicki AG, Zheng D, Frei SM, Wong GW, Hamadi S, Zhou S, Foster PS, Krilis SA, Stevens RL. Importance of mast cell Prss31/transmembrane tryptase/tryptase-gamma in lung function and experimental chronic obstructive pulmonary disease and colitis. *J Biol Chem* 2014: 289(26): 18214-18227.
10. Lu Z VEH, Liu G, Nair PM, Jones B, Gillis CM, Nalkurthi C, Verhamme F, Buyle-Huybrecht T, Vandenabeele P, Vanden Berghe T, Brusselle GG, Murphy JM, Wark PA, Bracke KR, Fricker M, Hansbro PM. Necroptosis signalling promotes inflammation, airway remodelling and emphysema in COPD. *American Journal of Respiratory and Critical Care Medicine* 2021: accepted 4.5.21.
11. Starkey MR, Plank MW, Casolari P, Papi A, Pavlidis S, Guo Y, Cameron GJM, Haw TJ, Tam A, Obiedat M, Donovan C, Hansbro NG, Nguyen DH, Nair PM, Kim RY, Horvat JC, Kaiko GE, Durum SK, Wark PA, Sin DD, Caramori G, Adcock IM, Foster PS, Hansbro PM. IL-22 and its receptors are increased in human and experimental COPD and contribute to pathogenesis. *Eur Respir J* 2019: 54(1).
12. Stevens RL, McNeil HP, Wensing LA, Shin K, Wong GW, Hansbro PM, Krilis SA. Experimental Arthritis Is Dependent on Mouse Mast Cell Protease-5. *J Biol Chem* 2017: 292(13): 5392-5404.
13. Pejler G, Ronnberg E, Waern I, Wernersson S. Mast cell proteases: multifaceted regulators of inflammatory disease. *Blood* 2010: 115(24): 4981-4990.
14. Beghdadi W, Madjene LC, Claver J, Pejler G, Beaudoin L, Lehuen A, Daugas E, Blank U. Mast cell chymase protects against renal fibrosis in murine unilateral ureteral obstruction. *Kidney Int* 2013: 84(2): 317-326.

15. Ahmad S, Wei CC, Tallaj J, Dell'Italia LJ, Moniwa N, Varagic J, Ferrario CM. Chymase mediates angiotensin-(1-12) metabolism in normal human hearts. *J Am Soc Hypertens* 2013: 7(2): 128-136.
16. Grashoff WF, Sont JK, Sterk PJ, Hiemstra PS, de Boer WI, Stolk J, Han J, van Krieken JM. Chronic obstructive pulmonary disease: role of bronchiolar mast cells and macrophages. *Am J Pathol* 1997: 151(6): 1785-1790.
17. Kosanovic D, Dahal BK, Peters DM, Seimetz M, Wygrecka M, Hoffmann K, Antel J, Reiss I, Ghofrani HA, Weissmann N, Grimminger F, Seeger W, Schermuly RT. Histological characterization of mast cell chymase in patients with pulmonary hypertension and chronic obstructive pulmonary disease. *Pulm Circ* 2014: 4(1): 128-136.
18. Kosanovic D, Luitel H, Dahal BK, Cornitescu T, Janssen W, Danser AH, Garrelds IM, De Mey JG, Fazzi G, Schiffers P, Iglarz M, Fischli W, Ghofrani HA, Weissmann N, Grimminger F, Seeger W, Reiss I, Schermuly RT. Chymase: a multifunctional player in pulmonary hypertension associated with lung fibrosis. *Eur Respir J* 2015: 46(4): 1084-1094.
19. Xu J, Xu X, Jiang L, Dua K, Hansbro PM, Liu G. SARS-CoV-2 induces transcriptional signatures in human lung epithelial cells that promote lung fibrosis. *Respir Res* 2020: 21(1): 182.
20. Hsu AC, Starkey MR, Hanish I, Parsons K, Haw TJ, Howland LJ, Barr I, Mahony JB, Foster PS, Knight DA, Wark PA, Hansbro PM. Targeting PI3K-p110alpha Suppresses Influenza Virus Infection in Chronic Obstructive Pulmonary Disease. *Am J Respir Crit Care Med* 2015: 191(9): 1012-1023.
21. Fricker M, Goggins BJ, Mateer S, Jones B, Kim RY, Gellatly SL, Jarnicki AG, Powell N, Oliver BG, Radford-Smith G, Talley NJ, Walker MM, Keely S, Hansbro PM. Chronic cigarette smoke exposure induces systemic hypoxia that drives intestinal dysfunction. *JCI Insight* 2018: 3(3).
22. Kim RY, Sunkara KP, Bracke KR, Jarnicki AG, Donovan C, Hsu AC, Ieni A, Beckett EL, Galvao I, Wijnant S, Ricciardolo FL, Di Stefano A, Haw TJ, Liu G, Ferguson AL, Palendira U, Wark PA, Conickx G, Mestdagh P, Brusselle GG, Caramori G, Foster PS, Horvat JC, Hansbro PM. A microRNA-21-mediated SATB1/S100A9/NF-kappaB axis promotes chronic obstructive pulmonary disease pathogenesis. *Sci Transl Med* 2021: 13(621): eaav7223.
23. Schanin J, Gebremeskel S, Korver W, Falahati R, Butuci M, Haw TJ, Nair PM, Liu G, Hansbro NG, Hansbro PM, Evensen E, Brock EC, Xu A, Wong A, Leung J, Bebbington C, Tomasevic N, Youngblood BA. A monoclonal antibody to Siglec-8 suppresses non-allergic airway inflammation and inhibits IgE-independent mast cell activation. *Mucosal Immunol* 2021: 14(2): 366-376.
24. Liu G, Cooley MA, Nair PM, Donovan C, Hsu AC, Jarnicki AG, Haw TJ, Hansbro NG, Ge Q, Brown AC, Tay H, Foster PS, Wark PA, Horvat JC, Bourke JE, Grainge CL, Argraves WS, Oliver BG, Knight DA, Burgess JK, Hansbro PM. Airway remodelling and inflammation in asthma are dependent on the extracellular matrix protein fibulin-1c. *J Pathol* 2017: 243(4): 510-523.
25. Skerrett-Byrne DA, Bromfield EG, Murray HC, Jamaluddin MFB, Jarnicki AG, Fricker M, Essilfie AT, Jones B, Haw TJ, Hampsey D, Anderson AL, Nixon B, Scott RJ, Wark PAB, Dun MD, Hansbro PM. Time-resolved proteomic profiling of cigarette smoke-induced experimental chronic obstructive pulmonary disease. *Respirology* 2021: 26(10): 960-973.
26. Pauwels RA, Buist AS, Calverley PM, Jenkins CR, Hurd SS. Global strategy for the diagnosis, management, and prevention of chronic obstructive pulmonary disease. NHLBI/WHO Global Initiative for Chronic Obstructive Lung Disease (GOLD) Workshop summary. *Am J Respir Crit Care Med* 2001: 163(5): 1256-1276.

27. Tilley AE, Harvey BG, Heguy A, Hackett NR, Wang R, O'Connor TP, Crystal RG. Down-regulation of the notch pathway in human airway epithelium in association with smoking and chronic obstructive pulmonary disease. *Am J Respir Crit Care Med* 2009: 179(6): 457-466.
28. Steiling K, van den Berge M, Hijazi K, Florido R, Campbell J, Liu G, Xiao J, Zhang X, Duclos G, Drizik E, Si H, Perdomo C, Dumont C, Coxson HO, Alekseyev YO, Sin D, Pare P, Hogg JC, McWilliams A, Hiemstra PS, Sterk PJ, Timens W, Chang JT, Sebastiani P, O'Connor GT, Bild AH, Postma DS, Lam S, Spira A, Lenburg ME. A dynamic bronchial airway gene expression signature of chronic obstructive pulmonary disease and lung function impairment. *Am J Respir Crit Care Med* 2013: 187(9): 933-942.
29. Jiang J, Faiz A, Berg M, Carpaij OA, Vermeulen CJ, Brouwer S, Hesse L, Teichmann SA, Ten Hacken NHT, Timens W, van den Berge M, Nawijn MC. Gene signatures from scRNA-seq accurately quantify mast cells in biopsies in asthma. *Clin Exp Allergy* 2020: 50(12): 1428-1431.
30. Dwyer DF, Ordovas-Montanes J, Allon SJ, Buchheit KM, Vukovic M, Derakhshan T, Feng C, Lai J, Hughes TK, Nyquist SK, Giannetti MP, Berger B, Bhattacharyya N, Roditi RE, Katz HR, Nawijn MC, Berg M, van den Berge M, Laidlaw TM, Shalek AK, Barrett NA, Boyce JA. Human airway mast cells proliferate and acquire distinct inflammation-driven phenotypes during type 2 inflammation. *Sci Immunol* 2021: 6(56).
31. Soltani A, Ewe YP, Lim ZS, Sohal SS, Reid D, Weston S, Wood-Baker R, Walters EH. Mast cells in COPD airways: relationship to bronchodilator responsiveness and angiogenesis. *Eur Respir J* 2012: 39(6): 1361-1367.
32. Liu G, Philp AM, Corte T, Travis MA, Schilter H, Hansbro NG, Burns CJ, Eapen MS, Sohal SS, Burgess JK, Hansbro PM. Therapeutic targets in lung tissue remodelling and fibrosis. *Pharmacol Ther* 2021: 225: 107839.
33. Parameswaran N, Patial S. Tumor necrosis factor-alpha signaling in macrophages. *Crit Rev Eukaryot Gene Expr* 2010: 20(2): 87-103.
34. Churg A, Wang RD, Tai H, Wang X, Xie C, Wright JL. Tumor necrosis factor-alpha drives 70% of cigarette smoke-induced emphysema in the mouse. *Am J Respir Crit Care Med* 2004: 170(5): 492-498.
35. Minematsu N, Blumental-Perry A, Shapiro SD. Cigarette smoke inhibits engulfment of apoptotic cells by macrophages through inhibition of actin rearrangement. *Am J Respir Cell Mol Biol* 2011: 44(4): 474-482.
36. Caughey GH. Mast cell tryptases and chymases in inflammation and host defense. *Immunol Rev* 2007: 217: 141-154.
37. Xu X, Zhang D, Lyubynska N, Wolters PJ, Killeen NP, Baluk P, McDonald DM, Hawgood S, Caughey GH. Mast cells protect mice from Mycoplasma pneumonia. *Am J Respir Crit Care Med* 2006: 173(2): 219-225.
38. Bozinovski S, Vlahos R, Zhang Y, Lah LC, Seow HJ, Mansell A, Anderson GP. Carbonylation caused by cigarette smoke extract is associated with defective macrophage immunity. *Am J Respir Cell Mol Biol* 2011: 45(2): 229-236.
39. Aaron SD, Vandemheen KL, Maltais F, Field SK, Sin DD, Bourbeau J, Marciniuk DD, FitzGerald JM, Nair P, Mallick R. TNFalpha antagonists for acute exacerbations of COPD: a randomised double-blind controlled trial. *Thorax* 2013: 68(2): 142-148.
40. Gosman MM, Postma DS, Vonk JM, Rutgers B, Lodewijk M, Smith M, Luinge MA, Ten Hacken NH, Timens W. Association of mast cells with lung function in chronic obstructive pulmonary disease. *Respir Res* 2008: 9: 64.
41. Abonia JP, Friend DS, Austen WG, Jr., Moore FD, Jr., Carroll MC, Chan R, Afnan J, Humbles A, Gerard C, Knight P, Kanaoka Y, Yasuda S, Morokawa N, Austen KF, Stevens

RL, Gurish MF. Mast cell protease 5 mediates ischemia-reperfusion injury of mouse skeletal muscle. *J Immunol* 2005: 174(11): 7285-7291.
42. Theiss AL, Simmons JG, Jobin C, Lund PK. Tumor necrosis factor (TNF) alpha increases collagen accumulation and proliferation in intestinal myofibroblasts via TNF receptor 2. *J Biol Chem* 2005: 280(43): 36099-36109.
43. Bankova LG, Lezcano C, Pejler G, Stevens RL, Murphy GF, Austen KF, Gurish MF. Mouse mast cell proteases 4 and 5 mediate epidermal injury through disruption of tight junctions. *J Immunol* 2014: 192(6): 2812-2820.
44. Washko GR, Hunninghake GM, Fernandez IE, Nishino M, Okajima Y, Yamashiro T, Ross JC, Estepar RS, Lynch DA, Brehm JM, Andriole KP, Diaz AA, Khorasani R, D'Aco K, Sciurba FC, Silverman EK, Hatabu H, Rosas IO, Investigators CO. Lung volumes and emphysema in smokers with interstitial lung abnormalities. *N Engl J Med* 2011: 364(10): 897-906.
45. McNulty W, Usmani OS. Techniques of assessing small airways dysfunction. *Eur Clin Respir J* 2014: 1.
46. Jones B, Donovan C, Liu G, Gomez HM, Chimankar V, Harrison CL, Wiegman CH, Adcock IM, Knight DA, Hirota JA, Hansbro PM. Animal models of COPD: What do they tell us? *Respirology* 2017: 22(1): 21-32.
47. Suki B, Stamenovic D, Hubmayr R. Lung parenchymal mechanics. *Compr Physiol* 2011: 1(3): 1317-1351.
48. Bot I, Bot M, van Heiningen SH, van Santbrink PJ, Lankhuizen IM, Hartman P, Gruener S, Hilpert H, van Berkel TJ, Fingerle J, Biessen EA. Mast cell chymase inhibition reduces atherosclerotic plaque progression and improves plaque stability in ApoE-/- mice. *Cardiovasc Res* 2011: 89(1): 244-252.
49. Douaiher J, Succar J, Lancerotto L, Gurish MF, Orgill DP, Hamilton MJ, Krilis SA, Stevens RL. Development of mast cells and importance of their tryptase and chymase serine proteases in inflammation and wound healing. *Adv Immunol* 2014: 122: 211-252.

Figure legends

FIGURE 1. Chymase 1 (CMA1) mRNA levels, mast cells (MCs) and CMA1$^+$ MCs are increased in the lungs of COPD patients. a) Human *(h)CMA1* mRNA levels in bronchial biopsies from lung healthy controls (n=18), non-COPD smokers (n=18) and mild GOLD I-II COPD patients (n=18 for each group) in an existing microarray dataset (GSE8545). **b)** *hCMA1* mRNA levels were measured in bronchial biopsies from lung healthy controls (n=12), non-COPD smokers (n=12) and severe GOLD III-IV COPD patients (n=15) in another existing microarray dataset (GSE5058). **c)** *hCMA1* mRNA levels were measured in bronchial biopsies from lung healthy controls (n=73), non-COPD smokers (n=100), and mild GOLD I-II (n=67) and severe GOLD III-IV (n=15) COPD patients in another existing microarray dataset (GSE37147). **d**) *hCMA1* mRNA transcript levels in two combined datasets (GSE38974 and GSE69818) from lung tissues from controls (n=9), COPD patients with GOLD I (n=12), II (n=26), III (n=7) and IV (n=19). **e)** Correlation between *hCMA1* and MC signatures in combined single cell RNA-sequencing data (GSE38974 and GSE69818) from lung tissues from COPD patients with GOLD I (n=16), II (n=49), III (n=9) and IV (n=19). **f)** *hCMA1* mRNA transcript levels in lung tissues from never smokers (n=26), smokers without COPD (n=34) and COPD patients with GOLD II-IV (n=40) by qPCR. **g)** Human lung sections from healthy controls (n=6) and COPD patients (n=6) were stained with CMA1 by immunohistochemistry (sale bar=100μm in both 20x and 40x magnifications), **h)** and CMA1$^+$ mast cells were enumerated. Results are mean ± SEM. Statistical differences were determined using one-way ANOVA with Bonferroni post-test.

FIGURE 2. Mast cell (MC) numbers and mMCP5 proteins are increased in the lungs in experimental COPD. Mice were exposed to 8 weeks of cigarette smoke (CS), controls were exposed to normal air. **a)** Lung tissues were collected and stained with chloroacetate esterase

to identify degranulating MCs. Images were taken using light microscopy (left, low magnification, scale bar: 100μm; right, high magnification, scale bar: 20μm, black arrows indicate MCs, and red arrows indicated MC degranulation). **b)** Total MC numbers and **c**) percentage of degranulated MCs were enumerated in the whole lung sections stained with chloroacetate esterase. **d)** Total proteins were extracted from mouse lungs and mMCP5 protein was detected by immunoblot analysis. **e)** Fold change of densitometry of mMCP5 normalised to β-actin. **f)** Mouse lung sections stained with mMCP5 (green), mMCP6 (red) and nuclei stained with DAPI (blue) in experimental COPD by immunofluorescence. **g)** $mMCP5^+$ and **h)** $mMCP6^+$ MCs were enumerated. n=4-6. Results are mean ± SEM. Statistical differences were determined with student *t*-test. *P<0.05.

FIGURE 3. Genotyping and mMCP5 protein assessment of *mmcp5*$^{-/-}$ mice. a) Genomic DNA was obtained from the tails of wild type (WT) and *mmcp5*$^{-/-}$ C57BL/6 mice, and a previously described PCR approach was used to genotype the mice. **b)** Lung proteins were extracted from WT and *mmcp5*$^{-/-}$ mice and mMCP5 protein was detected by immunoblot. Bone marrow derived mast cells (mBMMCs) were generated from WT and *mmcp5*$^{-/-}$ mice. **c)** Some mBMMCs were cytospun onto histology slides and stained with chloroacetate esterase (scale bar: 200 μm; insert shows the expanded image of indicated region, scale bar: 50 μm). **d)** Other mBMMCs were stained with anti-mMCP5 antibody to evaluate their immunohistochemistry (scale bar: 200 μm; rectangle indicates high magnification area, scale bar: 50 μm). **e)** mBMMC lysates were extracted from WT and *mmcp5*$^{-/-}$ mice and mMCP5 protein was detected using SDS-PAGE immunoblot.

FIGURE 4. Targeted disruption of the *mmcp5* gene protects against cigarette smoke (CS)-induced inflammation in experimental COPD. WT and *mmcp5*$^{-/-}$ mice were exposed

to CS or normal air for 8 weeks. **a)** Differential inflammatory cell counts in bronchoalveolar lavage fluid. Relative mRNA levels that encode **b)** *Tnfa*, **c)** *Cxcl1*, **d)** *Tgfb1*, **e)** *Il33*, **f)** *Ccl2* and **g)** *Il12* to *Hprt* in mouse lungs by RT-qPCR. **h)** TNF-α protein levels were measured in mouse lungs by ELISA. n=5–6. Results are mean ± SEM. Statistical differences were determined using one-way ANOVA with Bonferroni post-test. *P<0.05, **P<0.01, ***P<0.001, ****P<0.0001 compared to normal air-exposed controls. #P<0.05, ##P<0.01, ###P<0.001, ####P<0.0001 compared to CS-exposed WT mice.

FIGURE 5. *mmcp5* disruption protects against cigarette smoke (CS)-induced small airway remodelling, emphysema-like alveolar enlargement and reduced MMP protein in experimental COPD. WT and mmcp5$^{-/-}$ mice were exposed to CS or normal air for 8 weeks. **a)** Collagen deposition around small airways in lung sections was assessed using Masson's Trichrome histochemistry (blue colour indicates collagen, scale bar: 50μm; inserts show expanded image of indicate region; scale bar: 15μm). **b)** Quantification of collagen area around the small airways normalised to the perimeter of the basement membrane. **c)** Mouse lung sections were stained with haematoxylin and eosin (H&E) (scale bar: 50μm; inserts show expanded image of indicate region; scale bar: 15μm), and **d**) quantification of epithelial thickness in the small airways normalised to the perimeter of the basement membrane. **e**) Mouse lung sections were stained with H&E (scale bar: 200μm) and **f)** emphysema-like alveolar enlargement was measured by assessment of alveolar diameter. n=5-6. **g)** Total proteins were extracted from the lungs and pro- and active MMP9 were detected by immunoblot. Fold change of densitometry of **h)** pro- and **i)** active MMP9 normalised to β-actin. n=4-6. Results are the mean ± SEM. Statistical differences were determined using one-way ANOVA with Bonferroni post-test. *P<0.05, **P<0.01 compared to normal air-exposed controls. #P<0.05, ##P<0.01, ###P<0.005 compared to CS-exposed WT mice.

FIGURE 6. *mmcp5* disruption protects against cigarette smoke (CS)-induced impaired lung function in experimental COPD. WT and *mmcp5*$^{-/-}$ mice were exposed to CS or normal air for 8 weeks. Lung function was measured in terms of **a)** transpulmonary resistance, **b)** lung volume, **c)** dynamic compliance and **d)** static lung compliance from pressure-volume loops. n=5-6. Results are the mean ± SEM. Statistical differences were determined using one-way ANOVA with Bonferroni post-test. *P<0.05, ***P<0.001 compared to normal air-exposed controls. #P<0.05 compared to CS-exposed WT mice.

FIGURE 7. Cigarette smoke induces CMA1 release from mast cells (MCs) that induces macrophage secretion of TNF-α. a) mBMMCs from WT mice were co-cultured with mouse macrophages (RAW264.7) and exposed to 5% CSE for 6, 12, 24 or 48h. TNF-α protein levels were measured in cell lysates. mBMMCs from WT and *mmcp5*$^{-/-}$ mice were co-cultured with mouse macrophages and exposed to 5% CSE for 24h. TNF-α protein levels were measured in **b)** cell lysates and **c)** supernatants. n=3-6. **d)** Alveolar macrophages were isolated from WT and *mmcp5*$^{-/-}$ mice with or without 5% CSE stimulation and TNF-α protein levels measured in cell lysates. **e)** Alveolar macrophages from WT mice were co-cultured with mBMMCs from WT and *mmcp5*$^{-/-}$ mice with or without 24h 5% CSE stimulation and TNF-α protein levels were measured in cell lysates. Human MCs (HMC-1) were challenged with 5% CSE or media for 24h and CMA1 protein was measured in **f)** cell lysates and **g)** supernatants by ELSIA, n=5-6. Human macrophages (THP-1 differentiated macrophage cell line) were challenged with recombinant human (h)CMA1 protein for 24h. **h)** TNF gene expression in cells by qPCR **i)** TNF protein levels in supernatant by ELISA. **j)** Pathway of MC CMA1/mMCP5 contribution to COPD. CS exposure increases MC numbers and degranulation to release CMA1/mMCP5 in the lungs. mMCP5 induces macrophage to

release TNF-α that leads to lung inflammation, small airway remodelling and empyema in COPD. Results are mean ± SEM. Statistical differences were determined using one-way ANOVA with Bonferroni post-test. *P<0.05, **P<0.01, ****P<0.001 compared to non-CSE exposed control WT cells. #P<0.05 compared to CSE-exposed mBMMCs from WT mice.

FIGURE 8. CMA1 inhibitor suppresses the hallmark features of experimental COPD. **a)** Bone marrow derived mast cells were challenged with cigarette smoke extract or media and treated with or without CMA1 inhibitor, TNF levels were assessed in cell lysates. WT mice were exposed to cigarette smoke (CS) for 8 weeks, controls were exposed to normal air. Some mice were treated with CMA1 inhibitor intranasally (i.n) from week 6 to 8 of CS exposure and vehicle-treated controls received an equal volume of PBS. **b)** Total leukocytes, **c**) macrophages, **d)** neutrophils and **e)** lymphocytes in bronchoalveolar lavage fluid (BALF). **f**) mouse lungs were stained with Sirius Red and Fast Green for collagen (scale bar =50μm) and **g)** collagen deposition around small airways was normalised to the perimeter of basement membrane. **h)** Mouse lung sections were stained with H&E (scale bar =50μm) and **i)** alveolar diameter was determined using mean linear intercept. Mouse lung function in terms of **j)** lung volume, **k)** dynamic compliance and **l)** static lung compliance from pressure-volume loops. n=8. Results are mean ± SEM. Statical differences were determined using one-way ANOVA with Bonferroni post-test. *P<0.05, **P<0.01, ***P<0.001, ****P<0.0001 compared to air-exposed controls. #P<0.05, ##P<0.01 compared to vehicle-treated CS-exposed controls.

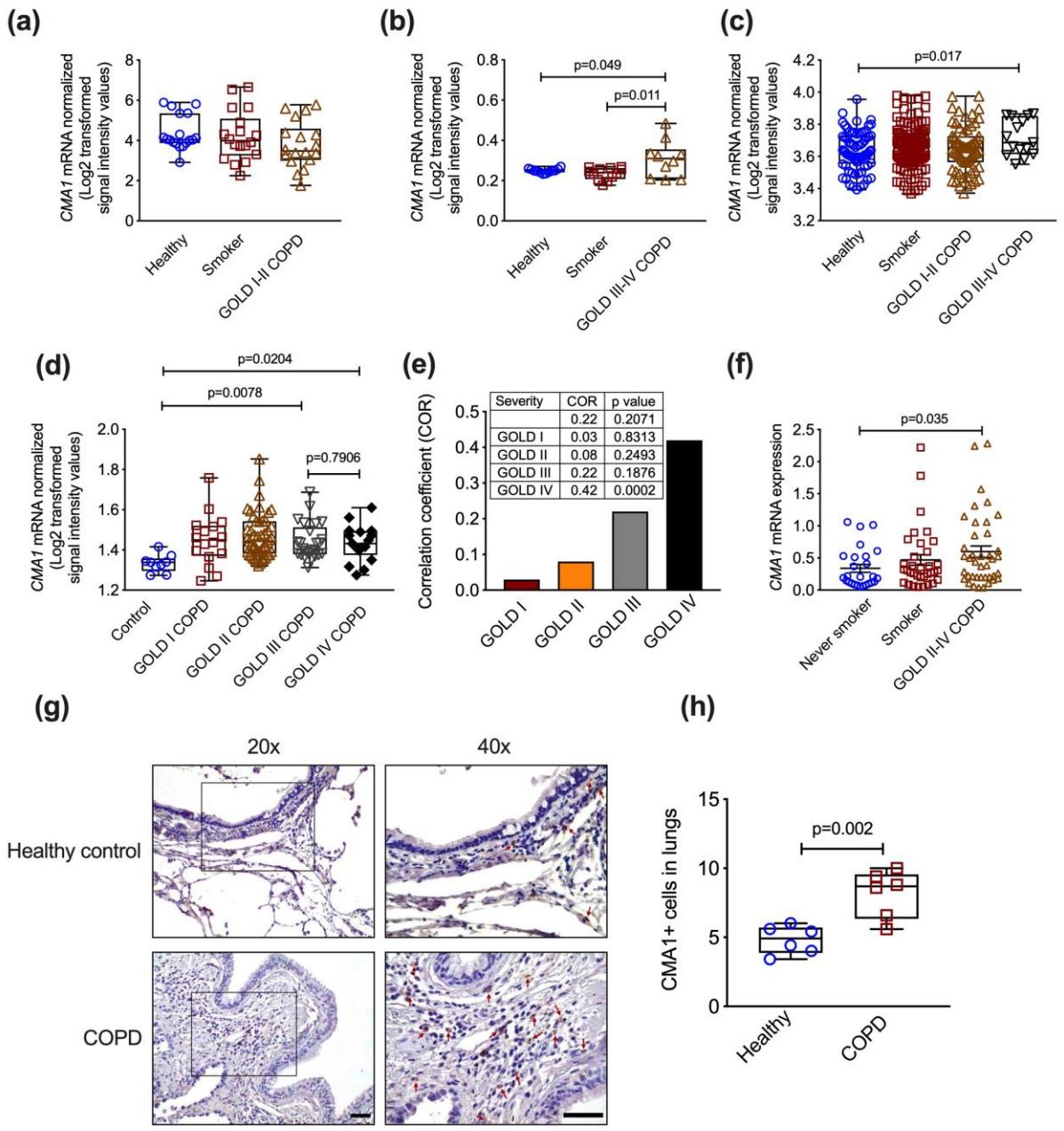
(a)
CMA1 mRNA normalized (Log2 transformed signal intensity values)
Healthy
Smoker
GOLD I-II COPD
(b)
p=0.049
p=0.011
GOLD III-IV COPD
(c)
p=0.017
(d)
p=0.0204
p=0.0078
p=0.7906
Control
GOLD I COPD
GOLD II COPD
GOLD III COPD
GOLD IV COPD
(e)
Correlation coefficient (COR)
Severity | COR | p value
0.22 | 0.2071
GOLD I | 0.03 | 0.8313
GOLD II | 0.08 | 0.2493
GOLD III | 0.22 | 0.1876
GOLD IV | 0.42 | 0.0002
(f)
CMA1 mRNA expression
p=0.035
Never smoker
(g)
20x
40x
Healthy control
COPD
(h)
CMA1+ cells in lungs
p=0.002

FIGURE 1

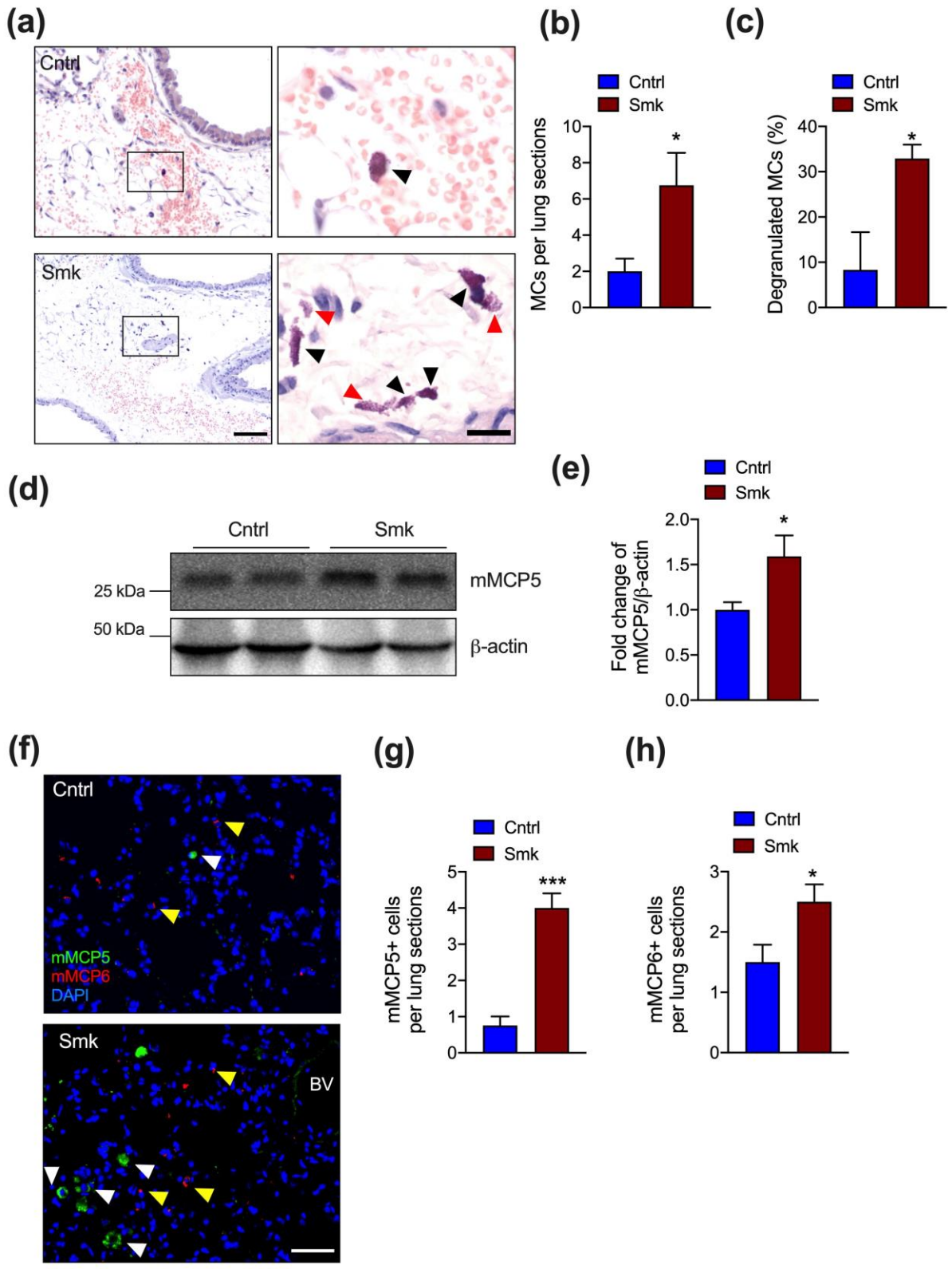
(a)
Cntrl
Smk
(b)
Cntrl
Smk
MCs per lung sections
(c)
Cntrl
Smk
Degranulated MCs (%)
(d)
Cntrl
Smk
25 kDa
50 kDa
mMCP5
β-actin
(e)
Cntrl
Smk
Fold change of mMCP5/β-actin
(f)
Cntrl
mMCP5
mMCP6
DAPI
Smk
BV
(g)
Cntrl
Smk
mMCP5+ cells per lung sections
(h)
Cntrl
Smk
mMCP6+ cells per lung sections

FIGURE 2

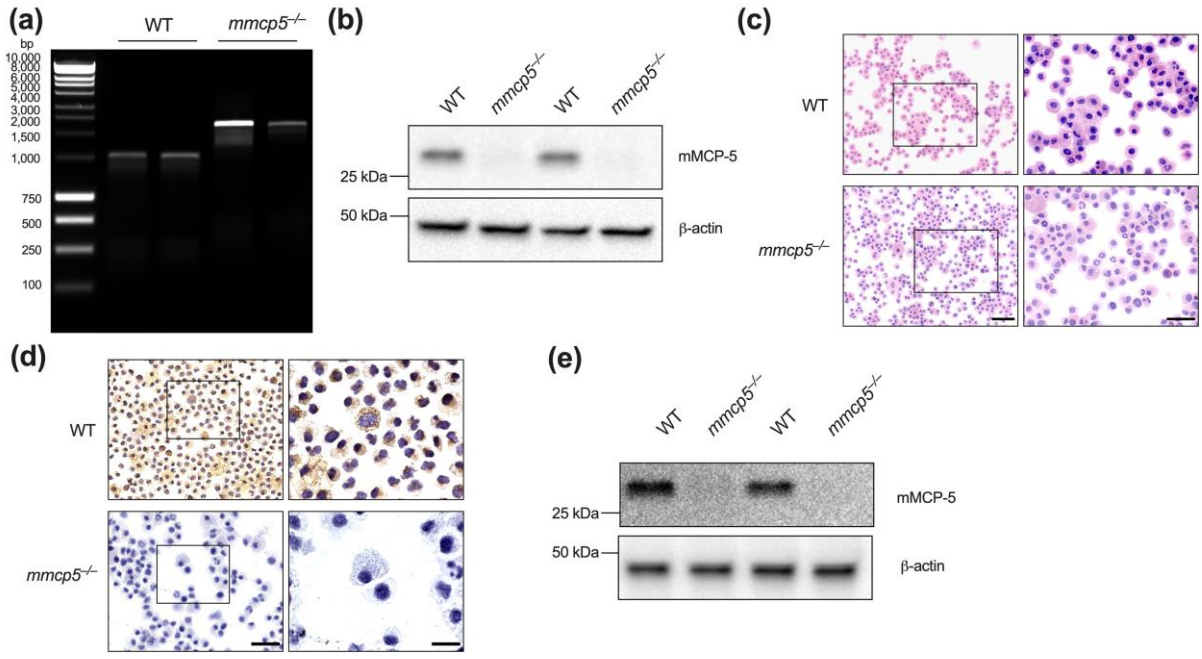
(a)
WT
mmcp5−/−
bp
10,000
8,000
6,000
5,000
4,000
3,000
2,000
1,500
1,000
750
500
250
100
(b)
WT
mmcp5−/−
WT
mmcp5−/−
25 kDa
50 kDa
mMCP-5
β-actin
(c)
WT
mmcp5−/−
(d)
WT
mmcp5−/−
(e)
WT
mmcp5−/−
WT
mmcp5−/−
25 kDa
50 kDa
mMCP-5
β-actin

FIGURE 3

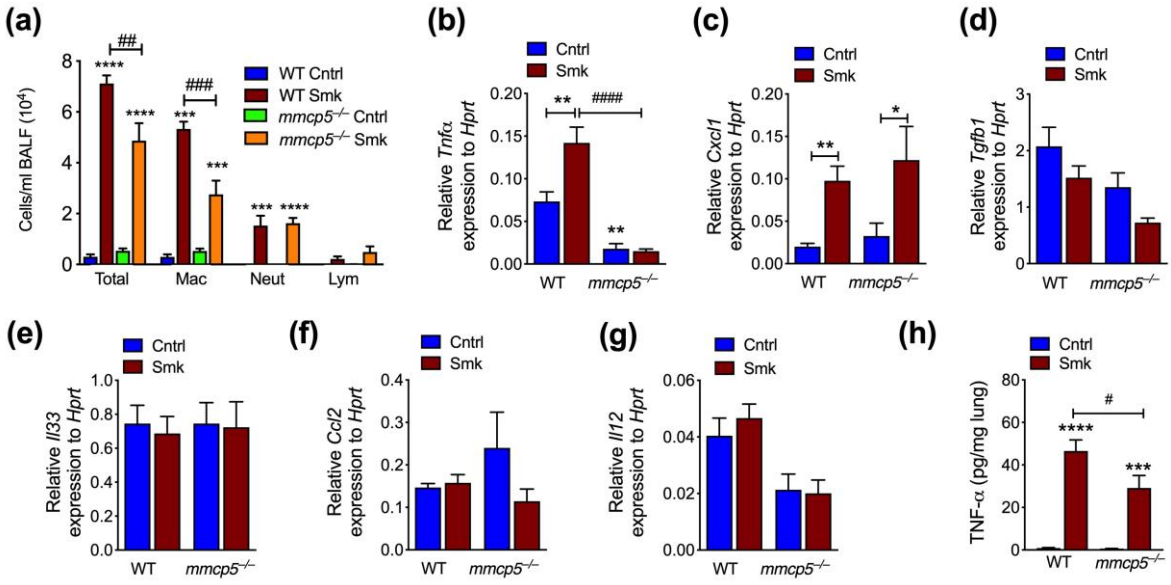
(a)
Cells/ml BALF (10^4)
WT Cntrl
WT Smk
mmcp5−/− Cntrl
mmcp5−/− Smk
Total
Mac
Neut
Lym
(b)
Relative Tnfα expression to Hprt
(c)
Relative Cxcl1 expression to Hprt
(d)
Relative Tgfb1 expression to Hprt
(e)
Relative Il33 expression to Hprt
(f)
Relative Ccl2 expression to Hprt
(g)
Relative Il12 expression to Hprt
(h)
TNF-α (pg/mg lung)
Cntrl
Smk
WT
mmcp5−/−

FIGURE 4

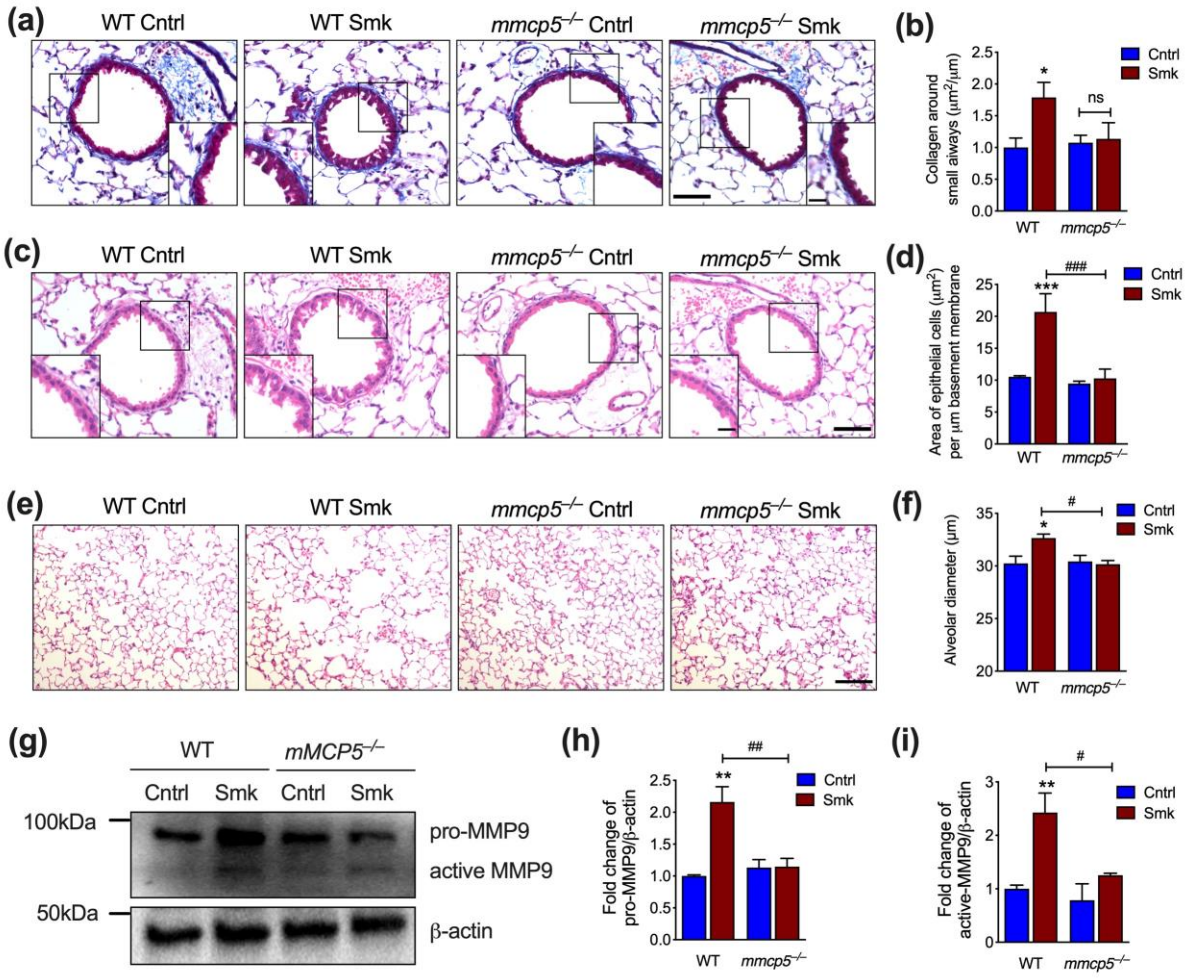
(a)
WT Cntrl
WT Smk
mmcp5−/− Cntrl
mmcp5−/− Smk
(b)
Collagen around small airways (μm²/μm)
Cntrl
Smk
*
ns
WT
mmcp5−/−
(c)
WT Cntrl
WT Smk
mmcp5−/− Cntrl
mmcp5−/− Smk
(d)
Area of epithelial cells (μm²) per μm basement membrane
###
***
Cntrl
Smk
WT
mmcp5−/−
(e)
WT Cntrl
WT Smk
mmcp5−/− Cntrl
mmcp5−/− Smk
(f)
Alveolar diameter (μm)
#
*
Cntrl
Smk
WT
mmcp5−/−
(g)
WT
mMCP5−/−
Cntrl
Smk
Cntrl
Smk
100kDa
pro-MMP9
active MMP9
50kDa
β-actin
(h)
Fold change of pro-MMP9/β-actin
##
**
Cntrl
Smk
WT
mmcp5−/−
(i)
Fold change of active-MMP9/β-actin
#
**
Cntrl
Smk
WT
mmcp5−/−

FIGURE 5

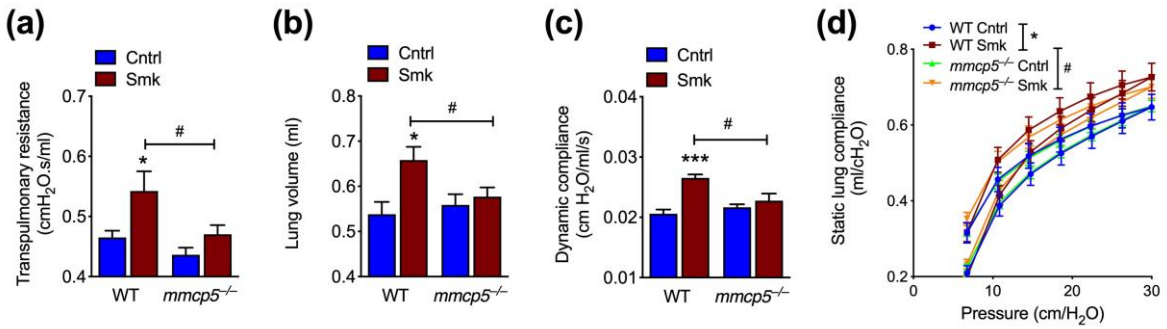
(a)
Cntrl
Smk
Transpulmonary resistance (cmH2O.s/ml)
0.7
0.6
0.5
0.4
*
#
WT
mmcp5−/−
(b)
Cntrl
Smk
Lung volume (ml)
0.8
0.7
0.6
0.5
0.4
*
#
WT
mmcp5−/−
(c)
Cntrl
Smk
Dynamic compliance (cm H2O/ml/s)
0.04
0.03
0.02
0.01
***
#
WT
mmcp5−/−
(d)
WT Cntrl
WT Smk
mmcp5−/− Cntrl
mmcp5−/− Smk
*
#
Static lung compliance (ml/cH2O)
0.8
0.6
0.4
0.2
0
10
20
30
Pressure (cm/H2O)

FIGURE 6

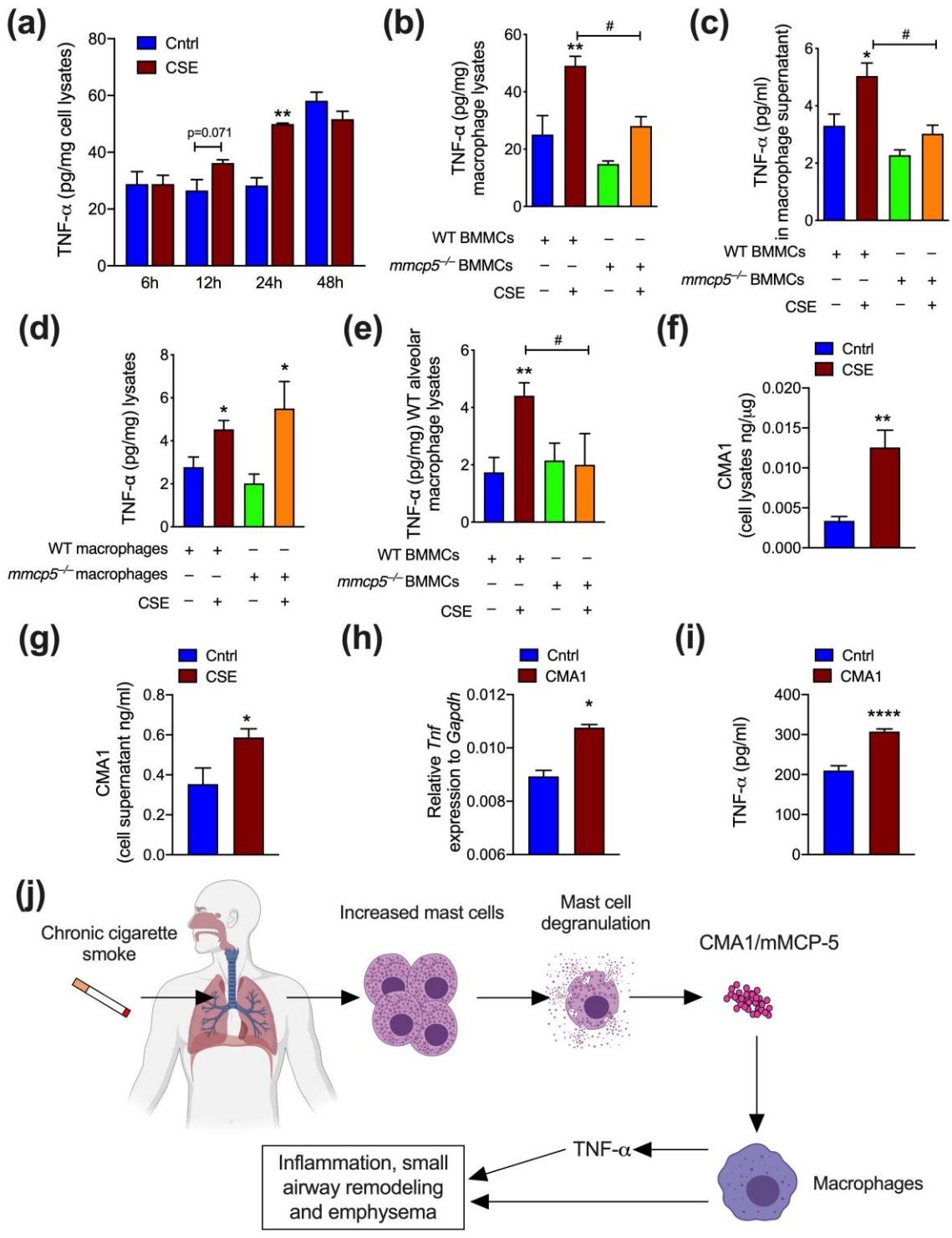
(a)
TNF-α (pg/mg cell lysates)
Cntrl
CSE
p=0.071
6h
12h
24h
48h
(b)
TNF-α (pg/mg) macrophage lysates
WT BMMCs
mmcp5−/− BMMCs
CSE
(c)
TNF-α (pg/ml) in macrophage supernatant
WT BMMCs
mmcp5−/− BMMCs
CSE
(d)
TNF-α (pg/mg) lysates
WT macrophages
mmcp5−/− macrophages
CSE
(e)
TNF-α (pg/mg) WT alveolar macrophage lysates
WT BMMCs
mmcp5−/− BMMCs
CSE
(f)
Cntrl
CSE
CMA1 (cell lysates ng/μg)
(g)
Cntrl
CSE
CMA1 (cell supernatant ng/ml)
(h)
Cntrl
CMA1
Relative Tnf expression to Gapdh
(i)
Cntrl
CMA1
TNF-α (pg/ml)
(j)
Chronic cigarette smoke
Increased mast cells
Mast cell degranulation
CMA1/mMCP-5
TNF-α
Macrophages
Inflammation, small airway remodeling and emphysema

FIGURE 7

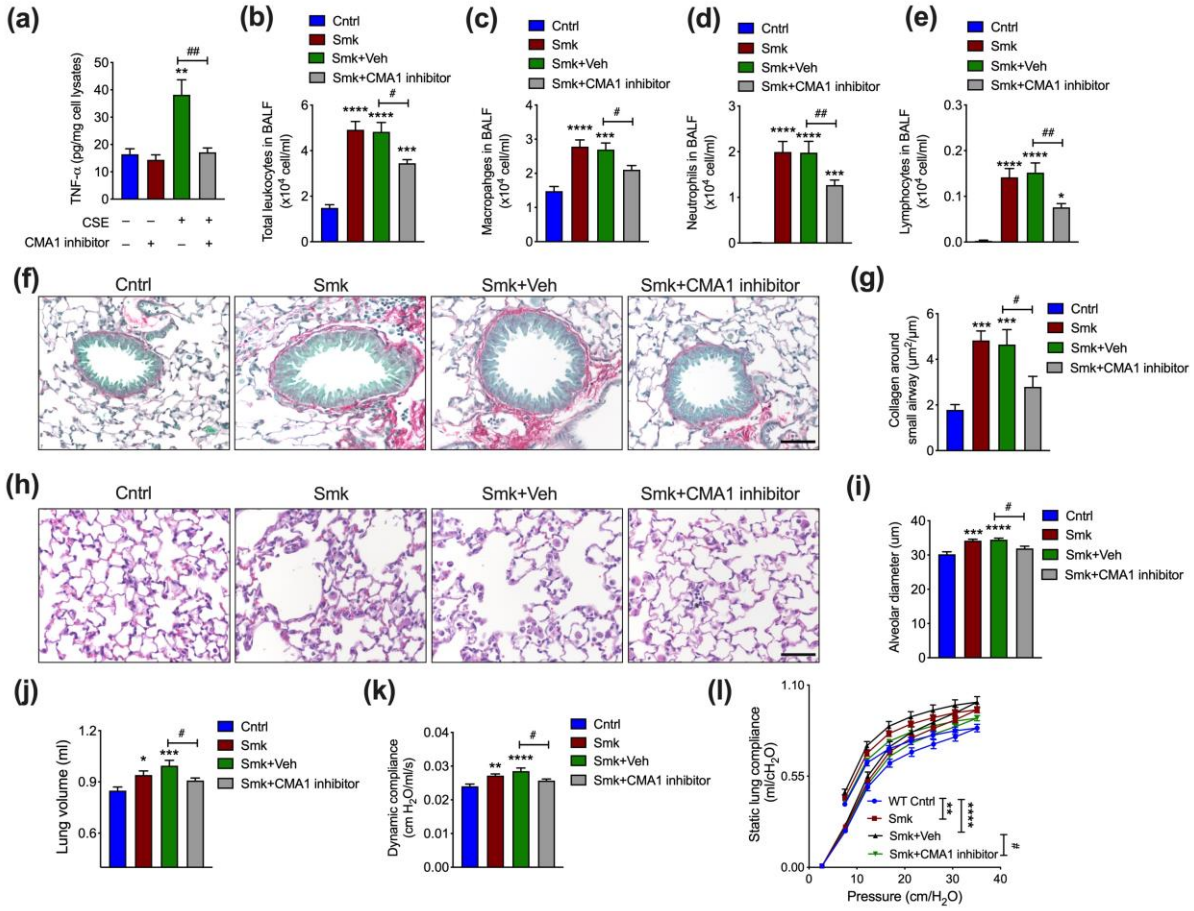
(a)
TNF-α (pg/mg cell lysates)
CSE
CMA1 inhibitor
(b)
Total leukocytes in BALF (x10⁴ cell/ml)
(c)
Macrophages in BALF (x10⁴ cell/ml)
(d)
Neutrophils in BALF (x10⁴ cell/ml)
(e)
Lymphocytes in BALF (x10⁴ cell/ml)
Cntrl
Smk
Smk+Veh
Smk+CMA1 inhibitor
(f)
(g)
Collagen around small airway (μm²/μm)
(h)
(i)
Alveolar diameter (um)
(j)
Lung volume (ml)
(k)
Dynamic compliance (cm H2O/ml/s)
(l)
Static lung compliance (ml/cH2O)
Pressure (cm/H2O)
WT Cntrl

FIGURE 8

Supplementary documents

Adverse roles of mast cell chymase-1 in chronic obstructive pulmonary disease

Gang Liu[1], Andrew G. Jarnicki[2], Keshav R. Paudel[1], Wenyinng Lu[3], Ridhima Wadhwa[1], Ashleigh M. Philp[1,4], Hannelore Van Eeckhoutte[5], Jacqueline E Marshall[1], Vamshikrishna Malyla[1], Angelica Katsifis[1], Michael Fricker[6], Nicole G. Hansbro[1], Kamal Dua[1,7], Nazanin Z. Kermani[8], Mathew S. Eapen[3], Angelica Tiotiu[9,10], K. Fan Chung[9], Gaetano Caramori[11], Ken Bracke[5], Ian M. Adcock[9], Sukhwinder S. Sohal[3], Peter A. Wark[6], Brian G. Oliver[11], Philip M. Hansbro[1,6*]

[1]Centre for Inflammation, Centenary Institute and University of Technology Sydney, School of Life Sciences, Faculty of Science, Sydney, New South Wales, Australia

[2]Department of Pharmacology and Therapeutics, University of Melbourne, Parkville, Victoria, Australia

[3]Department of Laboratory Medicine, School of Health Science, University of Tasmania, Launceston, Tasmania, Australia

[4]St Vincent's Medical School, University of New South Wale Medicine, University of New South Wale, Sydney, New South Wales, Australia

[5]Laboratory for Translational Research in Obstructive Pulmonary Diseases, Department of Respiratory Medicine, Ghent University Hospital, Ghent, Belgium.

[6]Priroity Research Centre for Healthy Lungs, Hunter Medical Research Institute, University of Newcastle, New South Wales, Australia

[7]Discipline of Pharmacy, Graduate School of Health, University of Technology Sydney, Ultimo, NSW, Australia

[8]Data Science Institute, Department of Computing, Imperial College London, United Kingdom

[9]National Heart & Lung Institute, Imperial College London, United Kingdom

[10]Department of Pulmonology, University Hospital of Nancy, France

[11]UOC di Pneumologia, Dipartimento di Scienze Biomediche, Odontoiatriche e delle Immagini Morfologiche e Funzionali (BIOMORF), Università di Messina, Italy.

[12]Woolcock Institute, School of Life Science, Faculty of Science Life science, University of Technology Sydney, Sydney, New South Wales, Australia

[*]Correspondence to: Professor Philip M Hansbro, Centre for Inflammation, Centenary Institute, Building 93, Royal Prince Alfred Hospital, John Hopkins Drive, Camperdown, NSW 2050, Australia. Email: philip.hansbro@uts.edu.au

Supplementary methods

Ethics statement

All experimental protocols were approved by Sydney Local Health District Animal Welfare Committee (2019/022 and 2019/037) and the Animal Ethics Committee of the University of Newcastle (A-2012-220).

Human samples and mRNA levels in microarrays

The levels of *hCMA1* mRNA transcripts were assessed using existing microarray datasets through Gene Expression Omnibus (GEO). The data were analysed with Array Studio software (Omicsoft Corporation, Research Triagnel Park, NC, USA), applying a general linear model adjusting for age and gender. The Benjamini–Hochberg method was used for P value adjustment [1-3]. To produce the GSE8545 dataset, bronchial (airway) biopsies were obtained from 18 non-smoking controls, 18 smokers without COPD and 18 smokers with mild GOLD I–II COPD (forced expiratory volume in 1 second [FEV_1] 50%-80%) classified according to GLOD criteria [4]. To produce the GSE5058 dataset, bronchial biopsies were obtained from 12 non-smoking controls, 12 smokers without COPD and 15 severe COPD patients with GOLD III-IV (FEV1< 50%) disease [5, 6]. For both these datasets, transcript levels were determined using Affymetrix Human Genome U133 Plus 2.0 Arrays. To produce the GSE37147 dataset, bronchial brushings were obtained from 73 lung healthy subjects, 100 smokers without COPD, 67 mild GOLD I-II COPD and 15 severe GOLD III-IV COPD patients, mRNA expression was profiled using Affymetrix Human Gene 1.0 ST Arrays [7]. *hCMA1* mRNA expression was mined in each of these datasets.

To assess *hCMA1* mRNA expression in COPD patients with different GOLD stages we combined two microarray datasets (GSE38974 and GSE69818). For GSE38974, lung tissues were collected from controls (n=9), COPD patients with GOLD I (n=7), II (n=9) and

IV (n=10), and mRNA expression was profiled using Agilent-014850 Whole Huma Genome microarray Affymetrix Human Gene 1.0 ST Arrays [8]. For GSE69818, lung tissues were obtained from COPD patients with GOLD I (n=5), II (n=17), III (n=7) and IV (n=9), and mRNA expression was profiled using Affymetrix Human Genome U133 Plus 2.0 Arrays [9].

Single cell (sc)RNA-sequencing analysis of total and CMA1$^+$ human MCs

We then assessed whether existing scRNA-seq data could be used to provide additional confirmation of increases in MCs and CMA1$^+$ MCs in COPD. We used existing scRNA-seq MC signatures as a measure of absolute MC numbers in asthma bronchial biopsies [10] and nasal polyps [11] and validated this data in a distinct cohort of asthma patients [12]. This showed that there was a good correlation between these scRNA-seq signatures and absolute MC numbers measured using anti-MC tryptase antibody (AA1) in bronchial biopsies (r=0.660, **Supplementary table 1**) and that this relationship was absent in sputum (not shown). The enrichment score for unstimulated MC signatures also correlated with sub-mucosal (r=0.326) MC numbers. The MC4 single cell signature from Dwyer et al. [11] correlated extremely well with sub-mucosal (r=0.756) MCs. The IL-4 stimulated signature also showed reasonable correlation with sub-mucosal (r=0.440) MC numbers. These signatures were used to identify MCs in COPD datasets.

These data indicate that scRNA-seq signatures are reasonable surrogates for MC counts in bronchial biopsies but not in other airway compartments such as sputum. We used therefore used the Jiang *et al.* [10] and Dwyer *et al.* [11] scRNA-seq signatures to examine enrichment in COPD lung datasets according to GOLD staging as they gave a reasonable reflection of MC numbers. MC signatures correlated with COPD disease severity and was highest for GOLD stage 4 (p=0.04 in GSE69818, **Supplementary table 2**). The correlation did not reach the significance in GSE38974 dataset due to smaller sample size.

hCMA1 mRNA transcript levels by qPCR

hCMA1 mRNA transcript levels were assessed in lung tissues from healthy controls (n=27), smokers without COPD (n=34) and COPD patients with GOLD II (n=38), III–IV (n=3) by qPCR (**Supplementary table 3**).

Immunohistochemistry

Surgically resected lung tissue from current smokers with COPD (COPD-CS, n=6) (Ethics ID: H0012374) and normal controls (NC, n=6) (Ethics ID: H00-50110) (James Hogg Lung Registry, the University of British Columbia) with donor characteristics into new **Supplementary table 4**. Tissues were cut at 3µm from paraffin-embedded blocks. Sections were incubated with CMA1 antibody (1:00 dilution, ab2377, Abcam, Australia) after incubation with heat retrieval solution (pH6, S169984, Dako, Victoria, Australia) in a decloaking chamber (110 °C, 15 mins), followed by peroxidase-conjugated polymer backbone that carries secondary antibody (EnVision™ detection systems, K5007, Dako, Victoria, Australia. Slides were incubated with DAB and images taken with a Leica camera and microscope (ICC50W, DM500) at 20x and 40x magnification brightfield.

For slides with mouse bone marrow derived mast cells (mBMMCs), they were incubated with citrate buffer (10 mM citric acid, 0.05% Tween-20, pH 6.0, 100 °C, 35 min) for antigen retrieval and blocked with 5% bovine serum albumin (Sigma-Aldrich, room temperature, 1 h). Slides were then incubated with 0.3% hydrogen peroxide (room temperature, 15 min) to block endogenous peroxidase. Anti-mMCP5-specific antibody in rabbits using a peptide approach was used as previously described [13]. Slides were incubated with mMCP5 antibody (1:1,000, 4°C overnight), and an anti-rabbit horseradish peroxidase-conjugated secondary antibody (R&D Systems) with visualisation by incubation

with Diaminobenzidine (DAB, DAKO, Agilent, US, room temperature, 8 min). Haematoxylin was used as a counterstain. Images were taken using an Axio Imager M2 microscope (Zeiss) as previously described [14].

mmcp5$^{-/-}$ mice and genotyping

We created *mmcp5*$^{-/-}$ mice on a C57BL/6 genetic background where the 5' to 3' region of exon 3 in the *mmcp5* gene was disrupted by inserting the Neo^{r} gene [13]. For genotyping, DNA was extracted from WT and *mmcp5*$^{-/-}$ mice using MyTaq^{TM} Extract-PCR kits (BIO-21126, Bioline) according to the manufacturer's instruction. Genotyping was achieved using PCR of genomic DNA (1 μg) and primers (5'-TCACTTGTCGGGATCTAC-3' and 5'-GGTTAGCTTGGCTTTTCTC-3') designed to amplify exon 3 of the *mmcp5* gene. Cycling of PCR was 30 cycles of 94 °C (1 min) for denaturation, 51 °C (1 min) for annealing step and 72 °C (2 min) for extension with a T100 PCR Thermal Cycler (Bio-rad). The DNA fragments of *mmcp5* from WT and *mmcp5*$^{-/-}$ mice were approximately 1 kb and 1.5 kb, respectively [13]. PCR products were separated at 100 V for 35 min using 1% agarose gel electrophoresis and visualised with a ChemiDoc MP system (Bio-Rad, Hercules, CA, USA).

CS-induced experimental COPD

Six-8 week old female WT and *mmcp5*$^{-/-}$ mice were exposed to the smoke of 12 3R4F cigarettes (University of Kentucky) using a custom-designed nose-only system, twice daily with 90 min rest in between, 5 times per week for 8 weeks as we have extensively described previously [14-25], including to study the role and potential for targeting of MCs [16, 17]. These exposures are equivalent to a pack-a-day human smoker [26, 27]. Age- and sex-matched control mice breathed normal air for the same time periods. All mice were

maintained under pathogen-free conditions. They were housed in the animal facility at the Australian BioResources, Centenary Institute and the University of Newcastle.

Some mice were treated intranasally (i.n) with 30 mg/kg of the CMA1 inhibitor RO5066852-000-006 (Roche, Australia) at least 2 hours before CS exposure, 5 days per week from week 6-8 of 8 weeks CS exposure. Control mice were vehicle treated with an equal volume of PBS.

MC staining

Mouse lungs were perfused, inflated, formalin fixed, and sectioned at 3 μm thickness. WT and *mmcp5*$^{-/-}$ mBMMCs [13, 28] were collected on histological slides after cytospin (300 x*g*, 10 min) [29, 30]. Both mouse lung sections and cell slides were stained with chloroacetate esterase, and the number of MCs were counted per mouse lung section [16, 31].

To quantify MCs, >50 images per lung section were taken using a light microscope (40x magnification), and MCs were enumerated. Five serial sections from each mouse lung were cut and stained with chloroacetate esterase to identify the location of degranulating MCs in the lungs.

mBMMCs generation

Bone marrow cells were collected from femurs and tibias of WT and *mmcp5*$^{-/-}$ mice, and mBMMCs were generated as described previously [13]. Bone marrow cells were flushed with RPMI-1640 media and centrifuged (112 x*g*, 4 °C, 10 min). Cells were then cultured in RPMI-1640 media supplemented with mouse recombinant interleukin (IL)-3 (R&D system), 10% fetal bovine serum, 2 mM L-glutamine, 0.1 mM non-essential amino acids, 100 U/ml penicillin and 100 μg streptomycin. Suspended cells were transferred to new flasks and fresh media added each week and 4-week mBMMCs were used in our studies. Total proteins were

extracted from mBMMCs lysates for SDS-PAGE immunoblot studies. Single cell suspension of other mBMMCs were prepared and separated by cytospin (300 x*g*, 10 min) for immunohistochemistry staining.

Protein extraction

For mouse lungs, tissues were homogenised in radioimmunoprecipitation assay (RIPA) buffer (R0278, Sigma-Aldrich, Macquarie Park, NSW, Australia) supplemented with PhosSTOP phosphatase inhibitor and complete protease inhibitor cocktails using a TissueLyser II (Qiagen, Hiden, Germany). For cells, lysates were obtained by scratching plates after adding RIPA buffer (100 μL). Total protein concentrations of mouse lungs or cell lysates were determined using BCA protein assay kits (Pierce Biotechnology, Thermo Fisher Scientific, Waltham, MA, USA) [32, 33].

Immunoblotting

Proteins were separated by SDS-PAGE and transferred to PVDF membranes [32, 34]. Blots were stained with mMCP5 (1: 1,000, NBP2-75441, Novus Biologicals, USA), MMP9 (1: 4,000, ab38898, Abcam, UK) or β-actin (1:10,000, ab8226, Abcam, Cambridge, UK, 4 °C, overnight) antibodies, and were incubated with anti-rabbit or anti-mouse secondary antibody (R&D system, Minneapolis, MN, USA, room temperature, 2h). Supersignal West Femto substrate (34095, ThermoFisher, USA) was used to detect proteins and images were taken with a ChemiDoc MP system (Bio-Rad, Hercules, CA, USA). Densitometry of proteins was measured using Image J (NIH, USA) and normalised to the density of control protein (β-actin). Values are presented as fold change of experimental groups compared to controls.

Immunofluorescence

Mouse lung sections were blocked (5% BSA, room temperature, 1h) and stained with anti-mouse CMA1 antibody (1:100, NBP2-75441, Novus Biologicals, 4°C, overnight), followed by anti-rabbit Alexa Fluor 488 secondary antibody (1:100, ab150077, Abcam, Australia, room temperature, 2h). Slides were stained with mMCP6 antibody (1:50, MAB3736, R&D Systems, 4°C, overnight) and incubated with anti-rat Alexa Fluor 594 secondary antibody (1:100, A-21209, ThermoFisher Scientific, room temperature, 2h). Slides were stained with DAPI for nuclei and images were taken using an Axio Imager M2 microscope (Zeiss).

BALF

BALF was obtained from mouse lungs by washing twice with 500 µl Hank's balanced salt solution (Sigma-Aldrich). Total cells were incubated with red cell lysis buffer (on ice, 5 min) and collected after centrifugation (125 x*g*, 4°C, 10 min). Cell were then transferred on histological slides by cytospin (300 x*g*, room temperature, 10 min). Slides were stained with May-Grunwald-Giemsa. Total cell numbers in BALF were determined using Trypan blue exclusion staining and a hemocytometer. and differential cell counts were enumerated using light microscopy [29, 35, 36].

RNA extraction and real-time quantitative (q)PCR

RNA was extracted from homogenised mouse lungs and livers using TRIzol^{TM} reagent (Invitrogen, Thermo Fisher Scientific) according to the manufacturer's instructions and concentrations of RNA was measured using a NanoDrop One^{C} (ThermoFisher Scientific) [33, 34]. RNA (1,000 ng) was reverse transcribed using reverse transcriptase (Bioscript, Bioline, London, UK) by RT-PCR. The primers for quantitative real-time PCR (qPCR) are provided in **Supplementary table 5** and the products were detected with SYBR reagents by qPCR (Bio-rad).

ELISA

TNF-α protein concentrations were determined in homogenised mouse lung tissues, cell lysates or supernatants by ELISA using a Duoset ELISA Development Systems (R&D systems, MN, USA) according to the manufacturer's instructions. Human CMA1 proteins were determined in cell lysates and supernatants using a hCMA1 ELISA kit (Cat# EKU03185, Biomatik, Canada) according to the manufacturer's instructions. The target proteins were normalised to total proteins [14, 23, 37].

Airway remodelling

Mouse lungs were perfused, inflated, formalin fixed and sectioned at 3–4 μm thickness. Slides were deparaffinised by serial passage twice in xylene and followed by a graded ethanol series. Slides were stained with Masson trichome for collagen. At least 6 small airways were randomly selected in each mouse lung and collagen deposition (blue colour) around the small airways was normalised to perimeter of airways. Slides were stained haematoxylin and eosin (H&E) for epithelial cell enlargement. Six small airways were randomly selected in each mouse lung and epithelial cell size in the small airways was normalised to the perimeter of the airways. Lung sections were stained with periodic acid-Schiff (PAS) for mucus, and the numbers of PAS-positive cells per 100 μm length of airways were enumerated [29]. The images were taken by a light microscope and evaluated by Image J as previously described [14, 17, 30].

Emphysema-like alveolar enlargement

Other mouse lung slides were stained with haematoxylin and eosin. Emphysema-like alveolar enlargements was assessed in lung parenchyma (exclude airways and blood vessels) using the mean linear intercept technique as previously described [14, 16, 17, 19, 30, 38].

Lung function

Mice were anaesthetised with a mix of xylazine (2 mg/ml) and ketamine (40 mg/ml), and cannulas were inserted into mouse tracheas by tracheostomy. Cannulas were connected to flexiVent apparatus (Legacy System; SCIREQ, Montreal, Canada). Lung functions in terms of transpulmonary resistance, lung volume, dynamic compliance and static lung compliance were assessed as previously described [14, 16, 17, 29, 30, 38, 39].

mBMMC and macrophage co-culture

Mouse macrophages (RAW264.5 cells, ATCC, TIB-71) were cultured in Dulbecco's Modified Eagle's Medium (DMEM) supplemented with 10% fetal bovine serum 10 mM HEPES and 2mM L-glutamine. Alveolar macrophages were isolated from the BALF of WT or mmcp5$^{-/-}$ mice [40]. BALF was collected through 10 PBS washes (1ml each) via a canula inserted into the trachea, and centrifugated (300 x*g*, 10 mins, 4°C). Resulting cells were incubated with red blood cell lysis buffer for 20 mins and then cultured in RPMI media (10% fetal bovine serum and penicillin/streptomycin) for 4h. Non-adherent cells were removed and alveolar macrophages were collected. The purity of macrophages was 92.4% of total cells (**Supplementary figure 7**) that was confirmed by flow cytometry.

Macrophages ($1x10^5$ cells/well) were seeded into 6-well plates for 24h. mBMMCs ($1x10^6$ cells/well) from WT and mmcp5$^{-/-}$ mice were added to wells containing macrophages and co-cultured (37 °C, 24h). CS from one cigarette was bubbled through 10 ml DMEM media to produce 100% CSE, and 5% CSE was prepared by dilution [41]. Co-cultured cells

were then exposed to 5% CSE and control cells were exposed to equal volumes of media only. Some cells were treated with 1μM CMA1 inhibitor compound RO5066852-000-006 (Roche, Australia) and control cells received an equal volume of culture media. Cell lysates or supernatant were collected after 6, 12, 24 and 48h of exposure for ELISA.

Flow cytometry

To assess the purity of alveolar macrophages, single cells were obtained from BALF from WT or *mmcp5*$^{-/-}$ mice and cultured in RPMI media for 4h. Cells were exposed to FC block and stained with DAPI for live/dead cells. The cells were stained with CD45 (AF700, BD Biosciences), F4/80 (APC, BD Biosciences) and SiglecF (BV421, BD Biosciences) and CD45^{+}F4/80^{+}siglecF^{+} macrophages were enumerated using a BD LSRFortessa (BD Biosciences). Data were analysed using FlowJO software (BD Biosciences) as described previously [34].

Human cell culture

Human MCs (HMC-1) were cultured in DMEM containing 10% fetal bovine serum, 10mM HEAPs, 2.5 mM L-glutamine and 1.2 mM α-thioglycerol. Cells (10^5) were seeded in a 24-well plate and some cells were challenged with 5% CSE for 24h. Control cells vehicle-challenged with an equal volume of culture media. Cell lysates were collected for ELISA.

Human monocytes (THP-1 cell line) were cultured in RPMI-1640 media containing 10% fetal calf serum, 2mM L-glutamine, 100nM penicillin/streptomycin. Cells were treated with 50 ng/ml phorbol 12 myristate 13 acetate (P8139, Sigma-aldrich) for 72h to differentiate monocytes into macrophages as previously described [42]. Macrophages were then challenged with recombinant hCMA1 protein (2.1μg/ml, C8118, Sigma-aldrich) and control

cells were challenged with an equal volume of cell media for 24h. RNA was extracted from the cells for qPCR, and cell supernatants were collected for ELISA.

Statistics

Results are presented as mean ± standard error of the mean (SEM) from mouse samples (n=6–8) from duplicate or triplicate experiments. Cell culture experiments were conducted in triplicated each time and were repeated at least three independent times. Comparisons between 2 groups were made using a Student's t-test, non-parametric test of Mann-Whitney U test or Fisher's exact test. Multiple comparisons (>2 groups) were made using one-way ANOVA with Bonferroni post-test using GraphPad Prism Software version 7 (San Diego, CA, USA). A P value <0.05 was considered significantly different.

Supplementary references

1. Li J, Xu X, Jiang Y, Hansbro NG, Hansbro PM, Xu J, Liu G. Elastin is a key factor of tumor development in colorectal cancer. *BMC Cancer* 2020: 20(1): 217.
2. Xu J, Xu X, Jiang L, Dua K, Hansbro PM, Liu G. SARS-CoV-2 induces transcriptional signatures in human lung epithelial cells that promote lung fibrosis. *Respir Res* 2020: 21(1): 182.
3. Ammous Z, Hackett NR, Butler MW, Raman T, Dolgalev I, O'Connor TP, Harvey BG, Crystal RG. Variability in small airway epithelial gene expression among normal smokers. *Chest* 2008: 133(6): 1344-1353.
4. Pauwels RA, Buist AS, Calverley PM, Jenkins CR, Hurd SS. Global strategy for the diagnosis, management, and prevention of chronic obstructive pulmonary disease. NHLBI/WHO Global Initiative for Chronic Obstructive Lung Disease (GOLD) Workshop summary. *Am J Respir Crit Care Med* 2001: 163(5): 1256-1276.
5. Carolan BJ, Heguy A, Harvey BG, Leopold PL, Ferris B, Crystal RG. Up-regulation of expression of the ubiquitin carboxyl-terminal hydrolase L1 gene in human airway epithelium of cigarette smokers. *Cancer Res* 2006: 66(22): 10729-10740.
6. Tilley AE, Harvey BG, Heguy A, Hackett NR, Wang R, O'Connor TP, Crystal RG. Down-regulation of the notch pathway in human airway epithelium in association with smoking and chronic obstructive pulmonary disease. *Am J Respir Crit Care Med* 2009: 179(6): 457-466.
7. Steiling K, van den Berge M, Hijazi K, Florido R, Campbell J, Liu G, Xiao J, Zhang X, Duclos G, Drizik E, Si H, Perdomo C, Dumont C, Coxson HO, Alekseyev YO, Sin D, Pare P, Hogg JC, McWilliams A, Hiemstra PS, Sterk PJ, Timens W, Chang JT, Sebastiani P, O'Connor GT, Bild AH, Postma DS, Lam S, Spira A, Lenburg ME. A dynamic bronchial airway gene expression signature of chronic obstructive pulmonary disease and lung function impairment. *Am J Respir Crit Care Med* 2013: 187(9): 933-942.
8. Ezzie ME, Crawford M, Cho JH, Orellana R, Zhang S, Gelinas R, Batte K, Yu L, Nuovo G, Galas D, Diaz P, Wang K, Nana-Sinkam SP. Gene expression networks in COPD: microRNA and mRNA regulation. *Thorax* 2012: 67(2): 122-131.
9. Faner R, Cruz T, Casserras T, Lopez-Giraldo A, Noell G, Coca I, Tal-Singer R, Miller B, Rodriguez-Roisin R, Spira A, Kalko SG, Agusti A. Network Analysis of Lung Transcriptomics Reveals a Distinct B-Cell Signature in Emphysema. *Am J Respir Crit Care Med* 2016: 193(11): 1242-1253.
10. Jiang J, Faiz A, Berg M, Carpaij OA, Vermeulen CJ, Brouwer S, Hesse L, Teichmann SA, Ten Hacken NHT, Timens W, van den Berge M, Nawijn MC. Gene signatures from scRNA-seq accurately quantify mast cells in biopsies in asthma. *Clin Exp Allergy* 2020: 50(12): 1428-1431.
11. Dwyer DF, Ordovas-Montanes J, Allon SJ, Buchheit KM, Vukovic M, Derakhshan T, Feng C, Lai J, Hughes TK, Nyquist SK, Giannetti MP, Berger B, Bhattacharyya N, Roditi RE, Katz HR, Nawijn MC, Berg M, van den Berge M, Laidlaw TM, Shalek AK, Barrett NA, Boyce JA. Human airway mast cells proliferate and acquire distinct inflammation-driven phenotypes during type 2 inflammation. *Sci Immunol* 2021: 6(56).
12. Tiotiu A, Badi Y, Kermani NZ, Sanak M, Kolmert J, Wheelock CE, Hansbro PM, Dahlen SE, Sterk PJ, Djukanovic R, Guo Y, Mumby S, Adcock IM, Chung KF, Team UBCP. Association of Differential Mast Cell Activation with Granulocytic Inflammation in Severe Asthma. *Am J Respir Crit Care Med* 2022: 205(4): 397-411.
13. Stevens RL, McNeil HP, Wensing LA, Shin K, Wong GW, Hansbro PM, Krilis SA. Experimental Arthritis Is Dependent on Mouse Mast Cell Protease-5. *J Biol Chem* 2017: 292(13): 5392-5404.

14. Liu G, Cooley MA, Jarnicki AG, Hsu AC, Nair PM, Haw TJ, Fricker M, Gellatly SL, Kim RY, Inman MD, Tjin G, Wark PA, Walker MM, Horvat JC, Oliver BG, Argraves WS, Knight DA, Burgess JK, Hansbro PM. Fibulin-1 regulates the pathogenesis of tissue remodeling in respiratory diseases. *JCI Insight* 2016: 1(9).
15. Franklin BS, Bossaller L, De Nardo D, Ratter JM, Stutz A, Engels G, Brenker C, Nordhoff M, Mirandola SR, Al-Amoudi A, Mangan MS, Zimmer S, Monks BG, Fricke M, Schmidt RE, Espevik T, Jones B, Jarnicki AG, Hansbro PM, Busto P, Marshak-Rothstein A, Hornemann S, Aguzzi A, Kastenmuller W, Latz E. The adaptor ASC has extracellular and 'prionoid' activities that propagate inflammation. *Nat Immunol* 2014: 15(8): 727-737.
16. Beckett EL, Stevens RL, Jarnicki AG, Kim RY, Hanish I, Hansbro NG, Deane A, Keely S, Horvat JC, Yang M, Oliver BG, van Rooijen N, Inman MD, Adachi R, Soberman RJ, Hamadi S, Wark PA, Foster PS, Hansbro PM. A new short-term mouse model of chronic obstructive pulmonary disease identifies a role for mast cell tryptase in pathogenesis. *J Allergy Clin Immunol* 2013: 131(3): 752-762.
17. Hansbro PM, Hamilton MJ, Fricker M, Gellatly SL, Jarnicki AG, Zheng D, Frei SM, Wong GW, Hamadi S, Zhou S, Foster PS, Krilis SA, Stevens RL. Importance of mast cell Prss31/transmembrane tryptase/tryptase-gamma in lung function and experimental chronic obstructive pulmonary disease and colitis. *J Biol Chem* 2014: 289(26): 18214-18227.
18. Tay HL, Kaiko GE, Plank M, Li J, Maltby S, Essilfie AT, Jarnicki A, Yang M, Mattes J, Hansbro PM, Foster PS. Antagonism of miR-328 increases the antimicrobial function of macrophages and neutrophils and rapid clearance of non-typeable Haemophilus influenzae (NTHi) from infected lung. *PLoS Pathog* 2015: 11(4): e1004549.
19. Jarnicki AG, Schilter H, Liu G, Wheeldon K, Essilfie AT, Foot JS, Yow TT, Jarolimek W, Hansbro PM. The inhibitor of semicarbazide-sensitive amine oxidase, PXS-4728A, ameliorates key features of chronic obstructive pulmonary disease in a mouse model. *Br J Pharmacol* 2016: 173(22): 3161-3175.
20. Hsu AC, Dua K, Starkey MR, Haw TJ, Nair PM, Nichol K, Zammit N, Grey ST, Baines KJ, Foster PS, Hansbro PM, Wark PA. MicroRNA-125a and -b inhibit A20 and MAVS to promote inflammation and impair antiviral response in COPD. *JCI Insight* 2017: 2(7): e90443.
21. Fricker M, Goggins BJ, Mateer S, Jones B, Kim RY, Gellatly SL, Jarnicki AG, Powell N, Oliver BG, Radford-Smith G, Talley NJ, Walker MM, Keely S, Hansbro PM. Chronic cigarette smoke exposure induces systemic hypoxia that drives intestinal dysfunction. *JCI Insight* 2018: 3(3).
22. Donovan C, Starkey MR, Kim RY, Rana BMJ, Barlow JL, Jones B, Haw TJ, Mono Nair P, Budden K, Cameron GJM, Horvat JC, Wark PA, Foster PS, McKenzie ANJ, Hansbro PM. Roles for T/B lymphocytes and ILC2s in experimental chronic obstructive pulmonary disease. *J Leukoc Biol* 2019: 105(1): 143-150.
23. Haw TJ, Starkey MR, Pavlidis S, Fricker M, Arthurs AL, Nair PM, Liu G, Hanish I, Kim RY, Foster PS, Horvat JC, Adcock IM, Hansbro PM. Toll-like receptor 2 and 4 have opposing roles in the pathogenesis of cigarette smoke-induced chronic obstructive pulmonary disease. *Am J Physiol Lung Cell Mol Physiol* 2018: 314(2): L298-L317.
24. Starkey MR, Plank MW, Casolari P, Papi A, Pavlidis S, Guo Y, Cameron GJM, Haw TJ, Tam A, Obiedat M, Donovan C, Hansbro NG, Nguyen DH, Nair PM, Kim RY, Horvat JC, Kaiko GE, Durum SK, Wark PA, Sin DD, Caramori G, Adcock IM, Foster PS, Hansbro PM. IL-22 and its receptors are increased in human and experimental COPD and contribute to pathogenesis. *Eur Respir J* 2019: 54(1).
25. Lu Z VEH, Liu G, Nair PM, Jones B, Gillis CM, Nalkurthi C, Verhamme F, Buyle-Huybrecht T, Vandenabeele P, Vanden Berghe T, Brusselle GG, Murphy JM, Wark PA, Bracke KR, Fricker M, Hansbro PM. Necroptosis signalling promotes inflammation, airway

remodelling and emphysema in COPD. *American Journal of Respiratory and Critical Care Medicine* 2021: accepted 4.5.21.
26. Fricker M, Deane A, Hansbro PM. Animal models of chronic obstructive pulmonary disease. *Expert Opin Drug Discov* 2014: 9(6): 629-645.
27. Jones B, Donovan C, Liu G, Gomez HM, Chimankar V, Harrison CL, Wiegman CH, Adcock IM, Knight DA, Hirota JA, Hansbro PM. Animal models of COPD: What do they tell us? *Respirology* 2017: 22(1): 21-32.
28. Levi-Schaffer F, Austen KF, Gravallese PM, Stevens RL. Coculture of interleukin 3-dependent mouse mast cells with fibroblasts results in a phenotypic change of the mast cells. *Proc Natl Acad Sci U S A* 1986: 83(17): 6485-6488.
29. Liu G, Cooley MA, Nair PM, Donovan C, Hsu AC, Jarnicki AG, Haw TJ, Hansbro NG, Ge Q, Brown AC, Tay H, Foster PS, Wark PA, Horvat JC, Bourke JE, Grainge CL, Argraves WS, Oliver BG, Knight DA, Burgess JK, Hansbro PM. Airway remodelling and inflammation in asthma are dependent on the extracellular matrix protein fibulin-1c. *J Pathol* 2017: 243(4): 510-523.
30. Haw TJ, Starkey MR, Nair PM, Pavlidis S, Liu G, Nguyen DH, Hsu AC, Hanish I, Kim RY, Collison AM, Inman MD, Wark PA, Foster PS, Knight DA, Mattes J, Yagita H, Adcock IM, Horvat JC, Hansbro PM. A pathogenic role for tumor necrosis factor-related apoptosis-inducing ligand in chronic obstructive pulmonary disease. *Mucosal Immunol* 2016: 9(4): 859-872.
31. Zouikr I, Ahmed AF, Horvat JC, Beagley KW, Clifton VL, Ray A, Thorne RF, Jarnicki AG, Hansbro PM, Hodgson DM. Programming of formalin-induced nociception by neonatal LPS exposure: Maintenance by peripheral and central neuroimmune activity. *Brain Behav Immun* 2015: 44: 235-246.
32. Liu G, Cooley MA, Jarnicki AG, Borghui T, Nair PM, Tjin G, Hsu AC, Haw TJ, Fricker M, Harrison CL, Jones B, Hansbro NG, Wark PA, Horvat JC, Argraves WS, Oliver BG, Knight DA, Burgess JK, Hansbro PM. Fibulin-1c regulates transforming growth factor-β activation in pulmonary tissue fibrosis *JCI Insight* 2019.
33. Liu G, Mateer SW, Hsu A, Goggins BJ, Tay H, Mathe A, Fan K, Neal R, Bruce J, Burns G, Minahan K, Maltby S, Fricker M, Foster PS, Wark PAB, Hansbro PM, Keely S. Platelet activating factor receptor regulates colitis-induced pulmonary inflammation through the NLRP3 inflammasome. *Mucosal Immunol* 2019: 12(4): 862-873.
34. Liu G, Baird AW, Parsons MJ, Fan K, Skerrett-Byrne DA, Nair PM, Makanyengo S, Chen J, Neal R, Goggins BJ. Platelet activating factor receptor acts to limit colitis-induced liver inflammation. *The FASEB Journal* 2020.
35. Preston JA, Essilfie AT, Horvat JC, Wade MA, Beagley KW, Gibson PG, Foster PS, Hansbro PM. Inhibition of allergic airways disease by immunomodulatory therapy with whole killed Streptococcus pneumoniae. *Vaccine* 2007: 25(48): 8154-8162.
36. Thorburn AN, O'Sullivan BJ, Thomas R, Kumar RK, Foster PS, Gibson PG, Hansbro PM. Pneumococcal conjugate vaccine-induced regulatory T cells suppress the development of allergic airways disease. *Thorax* 2010: 65(12): 1053-1060.
37. Nair PM, Starkey MR, Haw TJ, Liu G, Horvat JC, Morris JC, Verrills NM, Clark AR, Ammit AJ, Hansbro PM. Targeting PP2A and proteasome activity ameliorates features of allergic airway disease in mice. *Allergy* 2017: 72(12): 1891-1903.
38. Hsu AC, Starkey MR, Hanish I, Parsons K, Haw TJ, Howland LJ, Barr I, Mahony JB, Foster PS, Knight DA, Wark PA, Hansbro PM. Targeting PI3K-p110alpha Suppresses Influenza Virus Infection in Chronic Obstructive Pulmonary Disease. *Am J Respir Crit Care Med* 2015: 191(9): 1012-1023.
39. Harris RS. Pressure-volume curves of the respiratory system. *Respir Care* 2005: 50(1): 78-98; discussion 98-79.

40. Busch CJ, Favret J, Geirsdottir L, Molawi K, Sieweke MH. Isolation and Long-term Cultivation of Mouse Alveolar Macrophages. *Bio Protoc* 2019: 9(14).
41. Thaikoottathil JV, Martin RJ, Zdunek J, Weinberger A, Rino JG, Chu HW. Cigarette smoke extract reduces VEGF in primary human airway epithelial cells. *Eur Respir J* 2009: 33(4): 835-843.
42. Jimenez-Duran G, Luque-Martin R, Patel M, Koppe E, Bernard S, Sharp C, Buchan N, Rea C, de Winther MPJ, Turan N, Angell D, Wells CA, Cousins R, Mander PK, Masters SL. Pharmacological validation of targets regulating CD14 during macrophage differentiation. *EBioMedicine* 2020: 61: 103039.

Supplementary table 1. Mast cell (MC) signatures in single cell RNA-sequencing data correlated with MC numbers.

	Sub-mucosal mast cells (AA1+ cells/mm^2)	Sputum mast cell (%)	Sputum mast cell (cell #)
scRNA-seq Mast cell (Nawijn) [10]	0.660	-0.436	-0.416
Unstimulated Mast cell signature	0.326	0.250	0.269
DWYER_IL4STIM_MC	0.440	-0.354	-0.325
DWYER_MC1	-0.034	-0.401	-0.389
DWYER_MC2	0.278	-0.535	-0.543
DWYER_MC3	-0.141	-0.400	-0.417
DWYER_MC4	0.756	-0.376	-0.339

Supplementary table 2. Mast cell signatures in single cell RNA-sequencing data increase with COPD severity

			Dwyer_IL4STIM_MC		Dwyer_MC2		Dwyer_MC4		JIANG MC	
		GOLD Stage	rho	p value	rho	p value	rho	p value	rho	p value
Lung	GSE38974	Normal (n=9)	0.43	0.25	-0.45	0.23	0.22	0.58	0.52	0.16
		1 (n=5)	-0.5	0.45	-0.9	0.08	0.3	0.68	-0.3	0.68
		2 (n=8)	-0.19	0.66	-0.02	0.98	-0.43	0.3	-0.29	0.5
		4 (n=10)	0.44	0.2	0.67	0.04*	0.53	0.12	0.41	0.25
Lung	GSE69818	1 (n=11)	-0.24	0.49	0.2	0.56	0.28	0.4	0.07	0.84
		2 (n=41)	0.36	0.02*	0.01	0.93	0.12	0.44	0.21	0.19
		3 (n=9)	-0.18	0.64	0.2	0.61	0.17	0.68	0.45	0.23
		4 (n=9)	0.68	0.05*	0.3	0.44	0.35	0.36	0.72	0.04*

Supplementary table 3. Patient characteristics for mRNA analysis (by qRT-PCR) (n = 100)

	Never smokers	**Smokers without COPD**	**COPD GOLD II-IV**
Number	26	34	40
Age (years)	65 (56-71)	61 (55-70)	65 (57-69)
Sex (male/female)	12/14	20/14	30/10
BMI	26 (23-28)	25 (21-28)	24 (21-29)
Smoking			
Current/ex-smoker	NA	20/14[#]	25/15[#]
Pack-years	NA	28 (15-42)[*]	42 (35-54)[*†]
Lung function			
FEV_1 post (L)	2.8 (2.3-3.1)	2.6 (2.1-3.2)	1.9 (1.5-2.2)[*†]
FEV_1 post (% predicted)	97 (91-112)	94 (91-110)	63 (52-73)[*†]
FEV_1/FVC post	78 (73-83)	75 (71-79)	54 (42-57)[*†]
DL_{CO} (% predicted)	88 (79-104)	84 (69-99)	58 (46-79)[*†]
K_{CO} (% predicted)	95 (92-114)	95 (78-107)	73 (57-105)[*†]
Medication			
ICS (yes/no)	4/22[#]	2/32[#]	22/18[#]
OCS (yes/no)	0/26[#]	2/32[#]	10/30[#]
SABA (yes/no)	0/26[#]	2/32[#]	10/30[#]
LABA (yes/no)	2/24[#]	2/32[#]	22/18[#]
SAMA (yes/no)	0/26[#]	2/32[#]	9/31[#]
LAMA (yes/no)	0/26[#]	2/32[#]	18/22[#]

FEV_1 (forced expiratory volume in 1 second); FVC (forced vital capacity); DL_{CO} (diffusing capacity of the lungs for carbon monoxide); ICS (inhaled corticosteroids); OCS (oral corticosteroids); SABA (short acting β2-agonists); LABA (long acting β2-agonists); SAMA (short acting muscarinic antagonists); LAMA (long-acting muscarinic antagonists); NA (not applicable). Data are presented as median (IQR). Mann-Whitney U test: [*] $P < 0.05$ versus never smokers, [†] $P < 0.05$ versus smokers without COPD. Fisher's exact test: [#] $P<0.01$

Supplementary table 4. Patient characteristics for mast cell immunohistochemistry

Groups	**HC**	**COPD-CS**
Subjects	6	6
GOLD I/ II	NA	2/4
Sex (F/M)	3/3	4/2
Age (median, range)	45, 35-63	65, 59-78
Smoking pack-years (mean ± SD)	NA	31.40 ± 18.02
FEV1/FVC% Post BD (mean ± SD)	NA	67.23 ± 2.996
FEF 25-75% (L/sec) Post BD (mean ± SD)	NA	36.00 ± 8.155

Abbreviations: HC- healthy normal control; COPD-CS, COPD current smoker; FEV1/FVC % Post BD- forced expiration / forced vital capacity% post bronchodilator; FEF 25-75% (L/sec) Post BD- forced expiratory flow at 25-75% post bronchodilator.

Supplementary table 5. Mouse RT-qPCR primers for transcript analyses

Gene	**Forward sequence**	**Reverse sequence**
Tnfa	TCTGTCTACTGAACTTCGGGGTGA	TTGTCTTTGAGATCCATGCCGTT
Cxcl1	GCTGGGATTCACCTCAAGAA	CTTGGGGACACCTTTTAGCA
Tgfb1	CCCGAAGCGGACTACTATGCTA	GGTAACGCCAGGAATTGTTGCTAT
Il33	CCTCCCTGAGTACATACAATGACC	GTAGTAGCACCTGGTCTTGCTCTT
Ccl2	GCTACAAGAGGATCACCAGCAG	GTCTGGACCCATTCCTTCTTGG
Il12	CAATCACGCTACCTCCTCTTTT	CAGCAGTGCAGGAATAATGTTTC
Hprt	AGGCCAGACTTTGTTGGATTTGAA	CAACTTGCGCTCATCTTAGGCTTT
mcpt1	AAAAACAGCATACATGGGAG	CATATGCAGAGATTCTGGTG
mcpt2	CAATAG GACAAGGAGATTCTG	TAATAGGAGATTCGGGTGAAG
mcpt4	CACTGTAGTGGAAGAGAAATC	GAGGAATTACATTCACAGAGG
mcpt5	GTATACAAGGGAGACTCTGG	CAGAGTTAATTCTCCCTCAAG

Supplementary figure legends

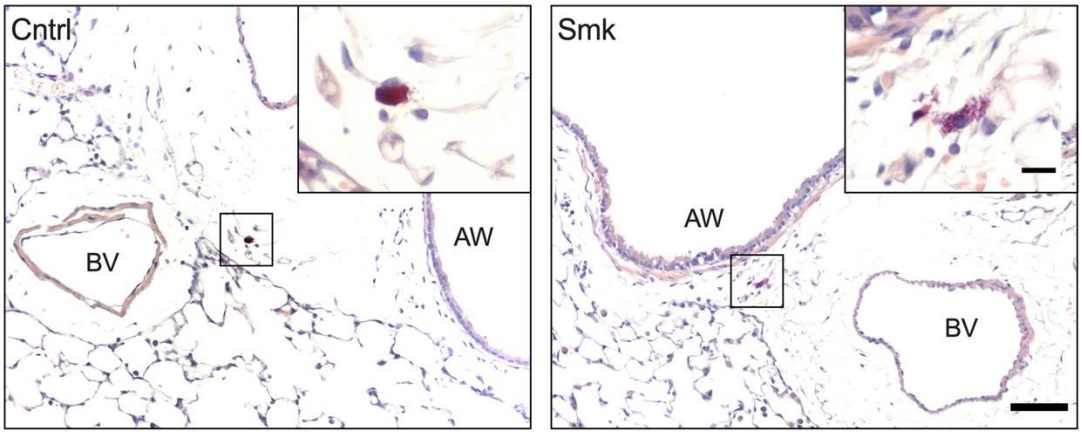

Supplementary figure 1. Mast cell (MC) localisation in experimental COPD. Mice were exposed to CS for 8 weeks to induce experimental COPD, control mice breathed normal air. Lungs were collected for histology and stained with chloroacetate esterase to identify degranulating MCs. BV=blood vessel; AW=airway. Scale bar=200μm. rectangle indicated expanded image, scale bar=20μm. The images were representative of 6 mice per group.

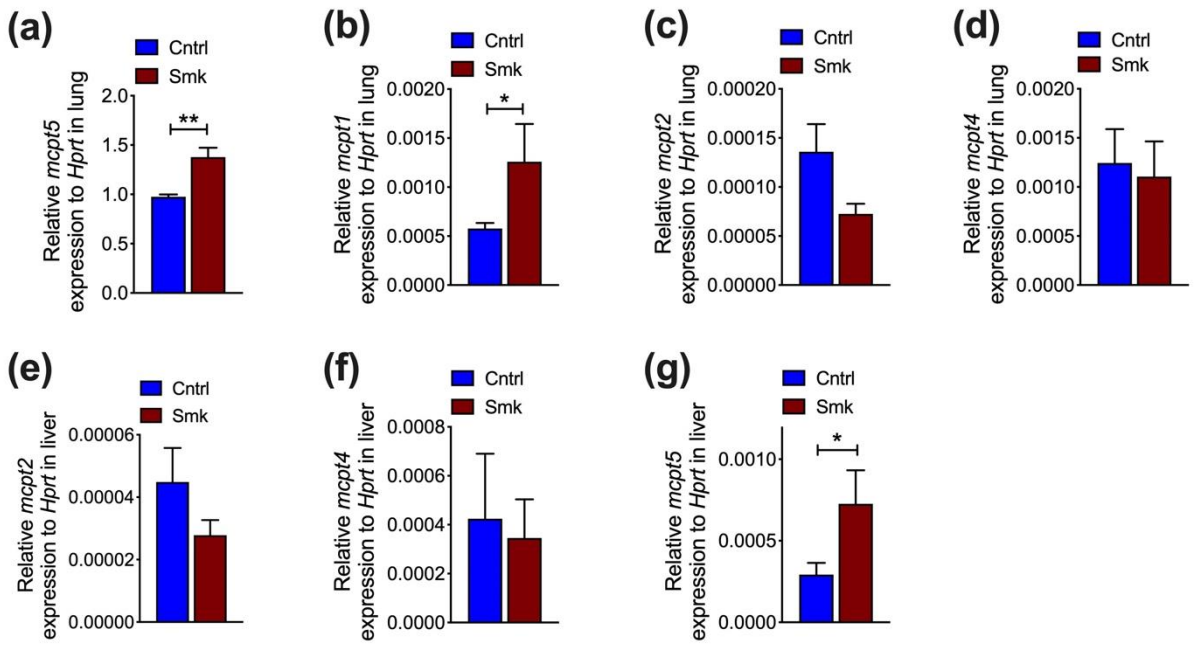

Supplementary figure 2. Mouse chymase gene expression in lungs and liver in experimental COPD. Mice were exposed to the smoke of 12 cigarettes, 2x per day, 5 days per week for 8 weeks, control mice breathed normal room air. **a)** *mcpt5*, **b)** *mcpt1*, **c)** *mcpt2* and **d)** *mcpt4* mRNA transcript levels in mouse lungs and **e)** *mcpt2*, **f)** *mcp41* and **g)** *mcpt5* mRNA transcript levels in mouse livers by qPCR. n=8. Results are mean ± SEM. Statical differences were determined using student t-test. *P<0.05, **P<0.01, compared to air-exposed controls.

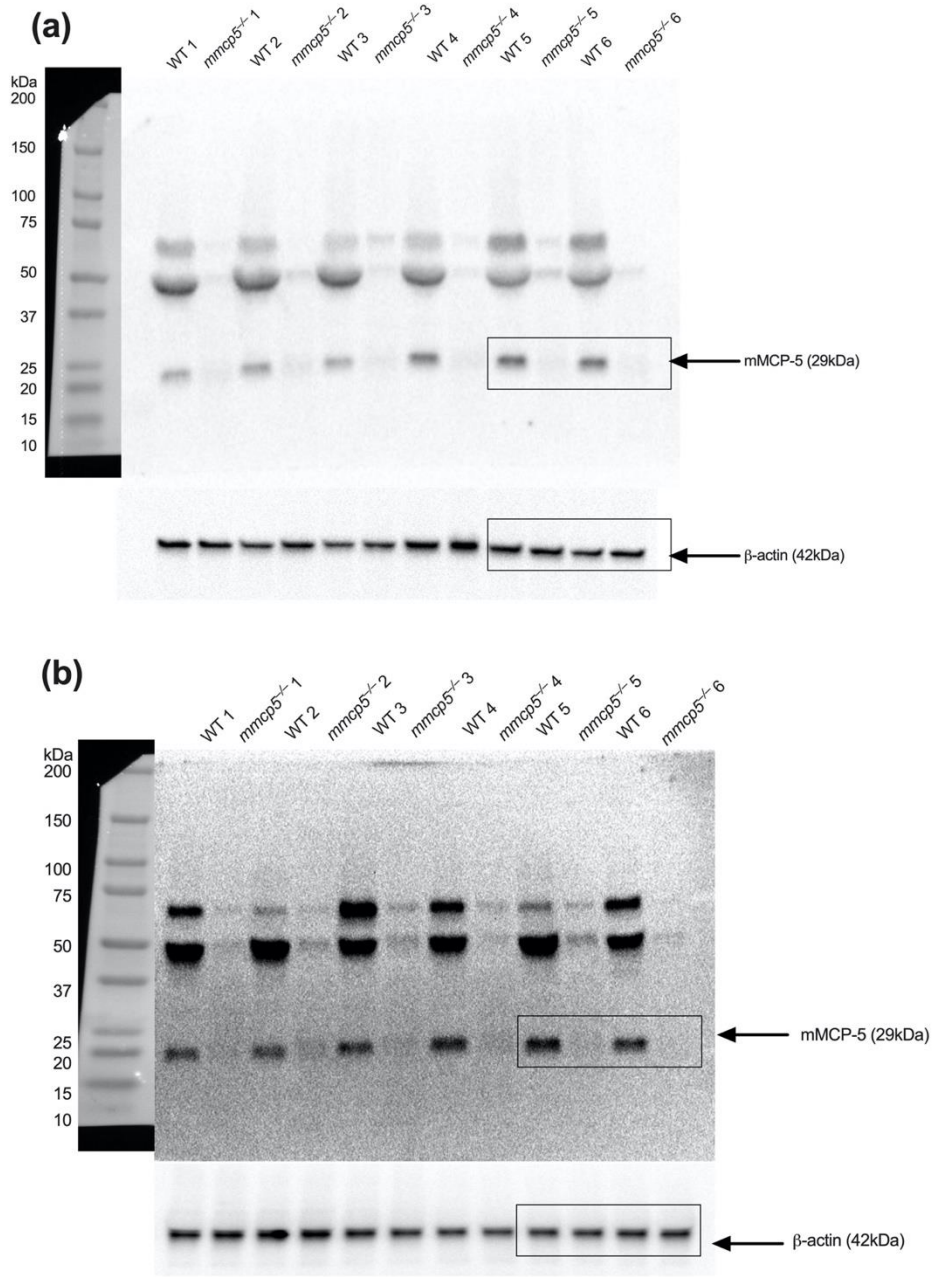

Supplementary figure 3. Immunoblots of mMCP5 and β-actin in Figure 3b and Figure 3e. Immunoblots were probed with anti-mMCP5 antibody. The same blots were washed and then re-probed with anti-β-actin antibody. **a)** mMCP5 protein in lung tissues from wild type (WT) and *mmcp5*$^{-/-}$ C57BL/6 mice, rectangles indicate the cropped representative image in **figure 3b**. **b)** mMCP5 protein in bone marrow-derived mast cell lysates from WT and *mmcp5*$^{-/-}$ mice, rectangles indicate the cropped representative image in **figure 3e**.

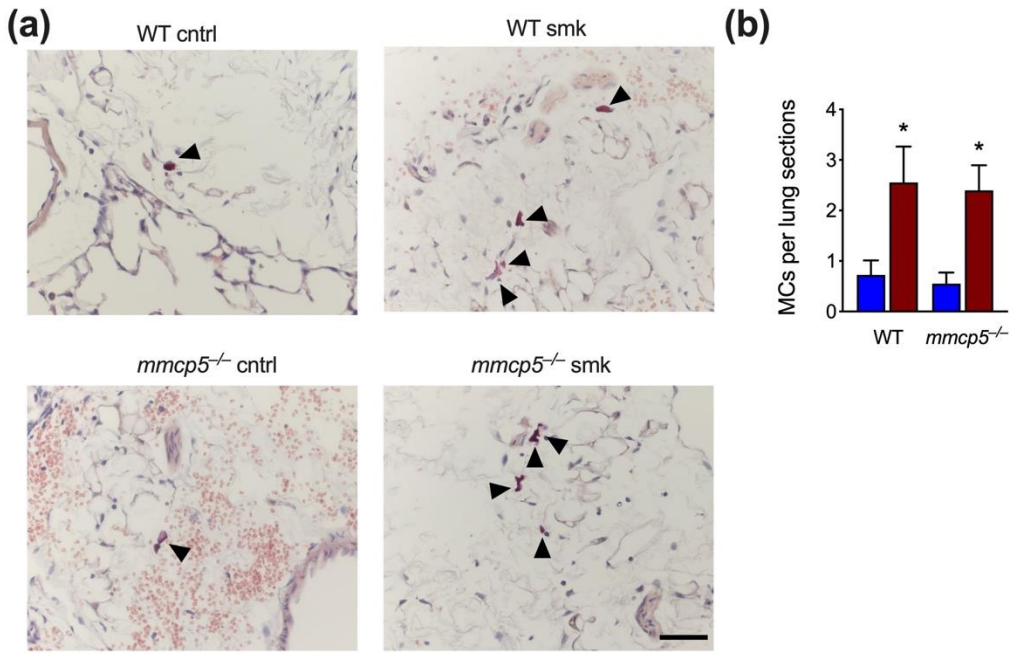

Supplementary figure 4. Mast cell (MC) density was not altered in the lungs after chronic cigarette smoke (CS) exposure. WT and mmcp5$^{-/-}$ mice were exposed to CS or normal air for 8 weeks. **a)** Mouse lung sections were stained with chloroacetate esterase for MCs. **b)** MCs were enumerated in the whole lung sections. Scale bar: 50 μm. n=4-6. Results are mean ± SEM. Statistical differences were determined with one-way ANOVA with Bonferroni post-test. *P<0.05 compared to air-exposed controls

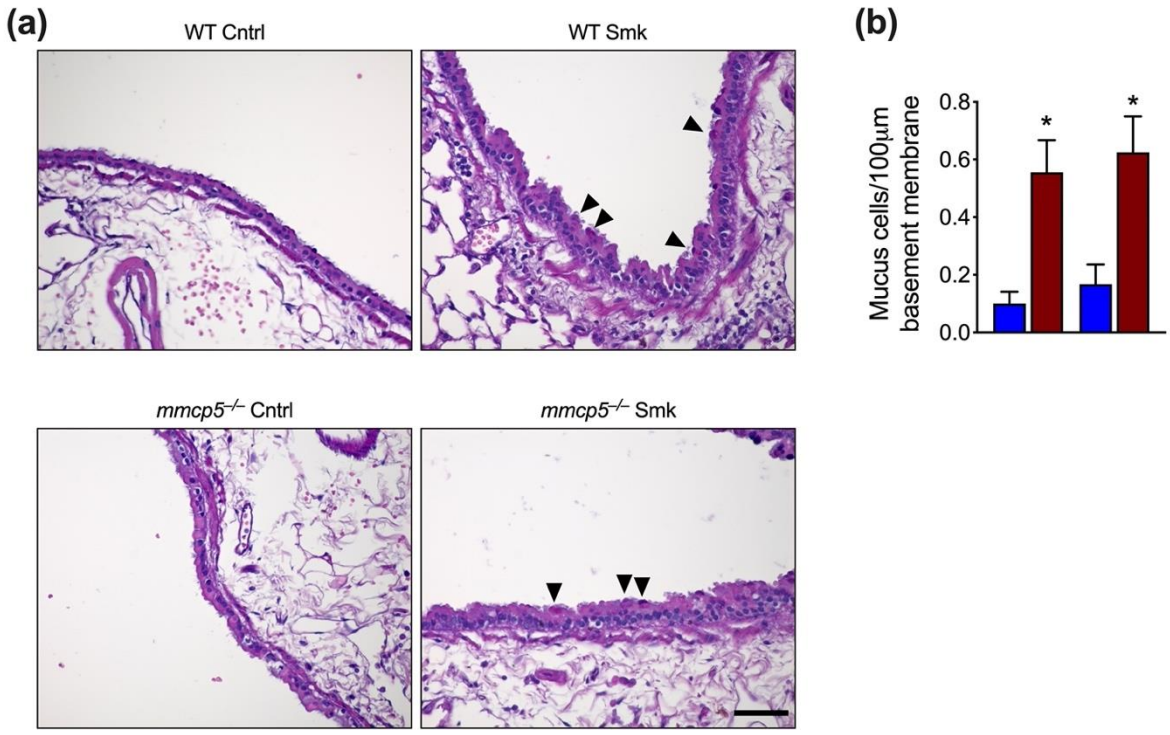

Supplementary figure 5: Mucus cells are increased in the lungs of WT and *mmcp5*$^{-/-}$ mice after chronic cigarette smoke (CS) exposure. WT and *mmcp5*$^{-/-}$ mice were exposed to CS or normal air for 8 weeks. **a)** Mouse lung sections were stain with periodic acid-schiff for mucus cells. **b)** Mucus secreting cells numbers were normalised to 100µm length of basement membrane in airways. Scale bar: 50 µm. n=4-6. Results are mean ± SEM. Statistical differences were determined with one-way ANOVA with Bonferroni post-test. *P<0.05 compared to normal air-exposed controls.

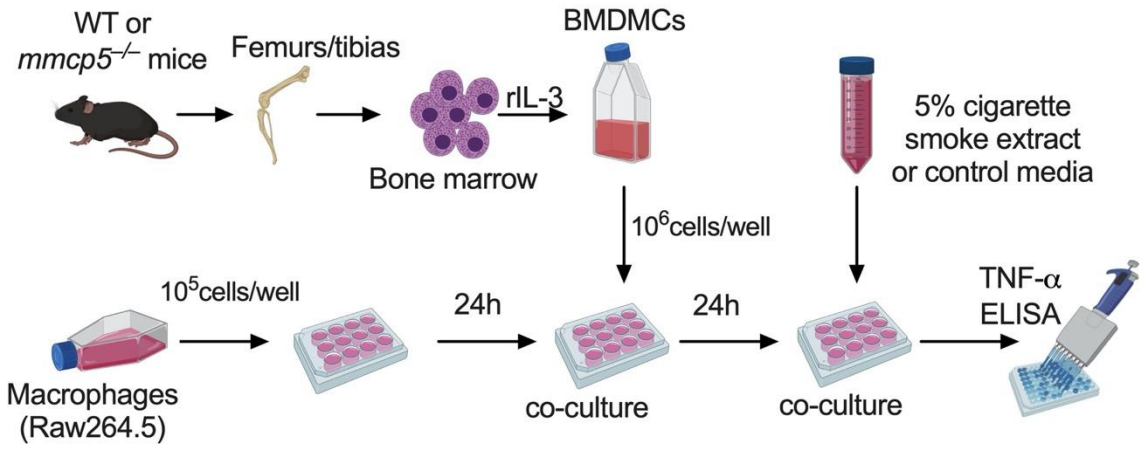

Supplementary figure 6. Cell culture experiment workflow. Bone marrow cells were isolated from WT or *mmcp5*$^{-/-}$ mice and bone marrow derived mast cells (mBMMCs) were differentiated and purified by culturing in media supplemented with recombinant mouse IL-3 (rIL-3). Macrophages (Raw264.5) cells were seeded on plates for 24h, and co-cultured with mBMMCs. CS extract (CSE, 5%) or control media were added to the cells, and TNF-α was measured in lysates by ELISA.

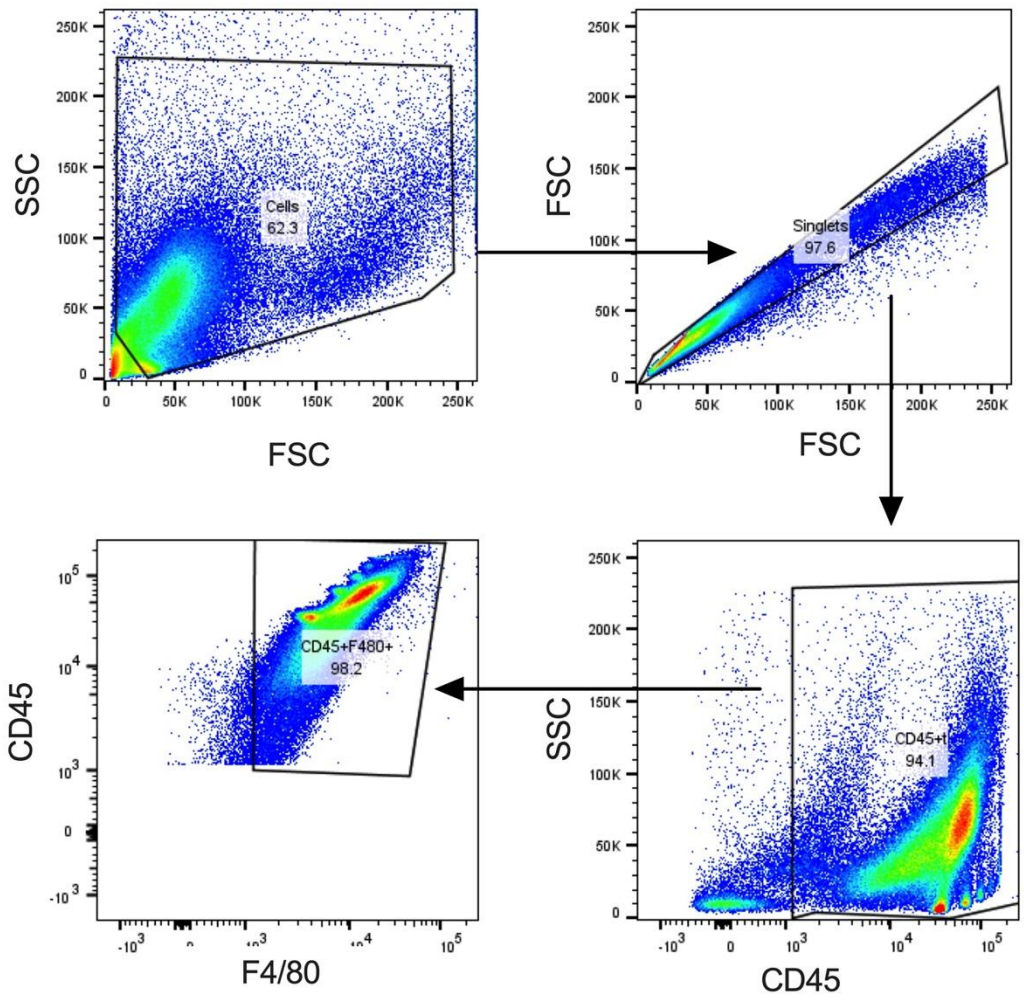

Supplementary figure 7. **Gating strategy for murine alveolar macrophages.** Cells were collected from mouse BALF and cultured in RPMI media for 4h. Adhesive cells were collected and stained with CD45 and F4/80 to assess macrophage purity. CD45+F4/80+ cells were enumerated by flow cytometry.